Electronic Supplementary Material (ESI) for ChemComm.

Supporting Information

Modulation of the Isomerization of ITI Switches by Supramolecular Confinement

Daniel Doellerer,[a] Ann-Kathrin Rückert,[b] Sandra Doria,[c,d] Michiel Hilbers,[e] Nadja A. Simeth,[f] Wybren Jan Buma,[e,g] Mariangela Di Donato,*[c,d] Ben L. Feringa,*[a] Wiktor Szymanski,*[a,h] & Stefano Crespi*[b]

[a] Stratingh Institute for Chemistry, Center for Systems Chemistry and Zernike Institute for Advanced Materials, Faculty of Mathematics and Natural Sciences, University of Groningen, Nijenborgh 4, 9747 AG Groningen, The Netherlands
[b] Department of Chemistry – Ångström Laboratory, Uppsala University, Box 523, 751 20 Uppsala, Sweden
[c] ICCOM-CNR, via Madonna del Piano 10, 50019 Sesto Fiorentino, Italy
[d] Laboratorio Europeo di Spettroscopia Non Lineare (LENS), via N. Carrara 1, 50019 Sesto Fiorentino, Italia
[e] Van 't Hoff Institute for Molecular Sciences, University of Amsterdam, Science Park 904, 1098 XH, Amsterdam, The Netherlands
[f] Institute for Organic and Biomolecular Chemistry, Department of Chemistry, University of Göttingen, Tammannstr. 2, 37077 Göttingen, Germany
[g] Institute for Molecules and Materials, FELIX Laboratory, Radboud University, Toernooiveld 7c, 6525 ED, Nijmegen, The Netherlands
[h] Medical Imaging Center, University Medical Center Groningen, University of Groningen, 9713 GZ Groningen, The Netherlands

E-mail: didonato@lens.unifi.it, b.l.feringa@rug.nl, w.c.szymanski@rug.nl & stefano.crespi@kemi.uu.se

Table of Contents

General Information

Chemicals were purchased from commercial sources, by name Sigma-Aldrich, Fluorochem, TCI and used without further purification. Dried solvents were obtained from Acros Organics or Alfa Aesar. If not stated otherwise, all reactions were carried out in oven-dried crimp top vials under a nitrogen atmosphere using standard Schlenk techniques. Solutions and reagents were added with nitrogen-flushed disposable syringes/needles. NMR spectra were recorded on a Varian Mercury-Plus 400, a Varian Unity Plus 500 or a Bruker 600 MHz NMR spectrometer at 298 K unless stated otherwise. Chemical shifts are reported in parts per million (ppm) and referenced to the residual solvent signal ($CDCl_3$: δ = 7.26 for ^1H and 77.2 for $^{13}C\{^1H\}$; $(CD_3)_2SO$: δ = 2.50 for ^1H and 39.5 for $^{13}C\{^1H\}$; D_2O: δ = 4.79 for ^1H) and thereby relatively stated to TMS. The resonance multiplicity is indicated as s = singlet, d = doublet, t = triplet, m = multiplet, dd = doublet of doublets, td = triplet of doublets, br = broad and the coupling constant values (*J*) are given in hertz (Hz). High resolution mass spectra (HRMS) were recorded on a LTQ Orbitrap XL spectrometer. UV-Vis absorption spectra were recorded on an Agilent 8453 UV-Vis Diode Array System, equipped with a Quantum Northwest Peltier controller in 10 mm quartz cuvettes. Irradiation experiments were performed using LEDs from Thorlabs Incorporated.

All compounds were synthesized according to modified literature procedures.[1–6] All spectra can be found in the appendix of the Supporting Information. **Cage** is 12+ positively charged and has 12 NO_3^- counterions which are omitted in most figures for clarity reasons.

In a control experiment, we investigated the possible partial solubility of the **ITI** in D_2O. **ITI** was suspended in D_2O under the same conditions as the encapsulation experiments. After 24 h, the undissolved **ITI** was filtered off over cotton wool and UV-Vis and NMR analysis of the solvent did not reveal any traces of **ITI** in the aqueous solution. We also explored the possibility of decomplexation of the **Cage** by the **ITI** molecule which could coordinate a Pd species, forming a separate complex under our experimental conditions. Therefore, **ITI** was added to a solution of Pd-precursor **2** in D_2O and the solution stirred for 24 h. It was concluded that **2** and **ITI** did not form a water-soluble complex as NMR analysis did not show any additional signals.

It is known from recent studies that **Cage** can assume two distinct conformations depending on the nature of the host, with a tubular form preferred for elongated guests (like **ITI**) and a more rigid shape for tetrahedrally shaped guests.[7] Upon encapsulation of ITI, we do not observe the typical third peak in the 9.0 ppm region of ^1H NMR for the encapsulated product in the second Cage isomer, hence we consider the tubular form as the dominant one. Although we anticipate the event of a molecular rearrangement of the cage in the ps timescale unlikely, we cannot completely rule out the possibility that the second excited state component derives from the interaction of the excited **ITI** with a different conformation of **Cage**. Regardless of the origin, it is evident that the molecular cage is effective in modulating the excited state lifetimes of **ITI**.

To obtain the weighted UV-Vis samples, **Cage** was dissolved in D_2O (c = ~3 x 10^{-3} M), **ITI** (1.0, 2.0, 3.0 and 10.0 eq.) added and the solutions stirred for 24 h at 250 rpm and 35 ºC. The solutions were then filtered over a glass pipette with cotton wool, extensively washed with D_2O, the remaining **ITI** dissolved in $CHCl_3$ and the obtained samples dried, weighted and the uptake compared to 1.0 eq.. The prior obtained solutions, were then subjected to UV-Vis analysis.

To prepare films of a sufficient optical density (OD ≥ 1) at the wavelengths of irradiation (400 nm), **ITI** (3.26 mg) was added to a 10 w/v% solution of PMMA (327 mg) in toluene. The solutions were homogenized through rapid stirring with a magnetic stirring bar in a sealed vial and then dropped on microscopy glass cuts to cast a homogeneous layer. The films were left drying at ambient conditions overnight. The OD was measured by UV-Vis absorption spectroscopy and suitable samples were selected for transient spectroscopy experiments.

Synthesis

Synthesis Schemes

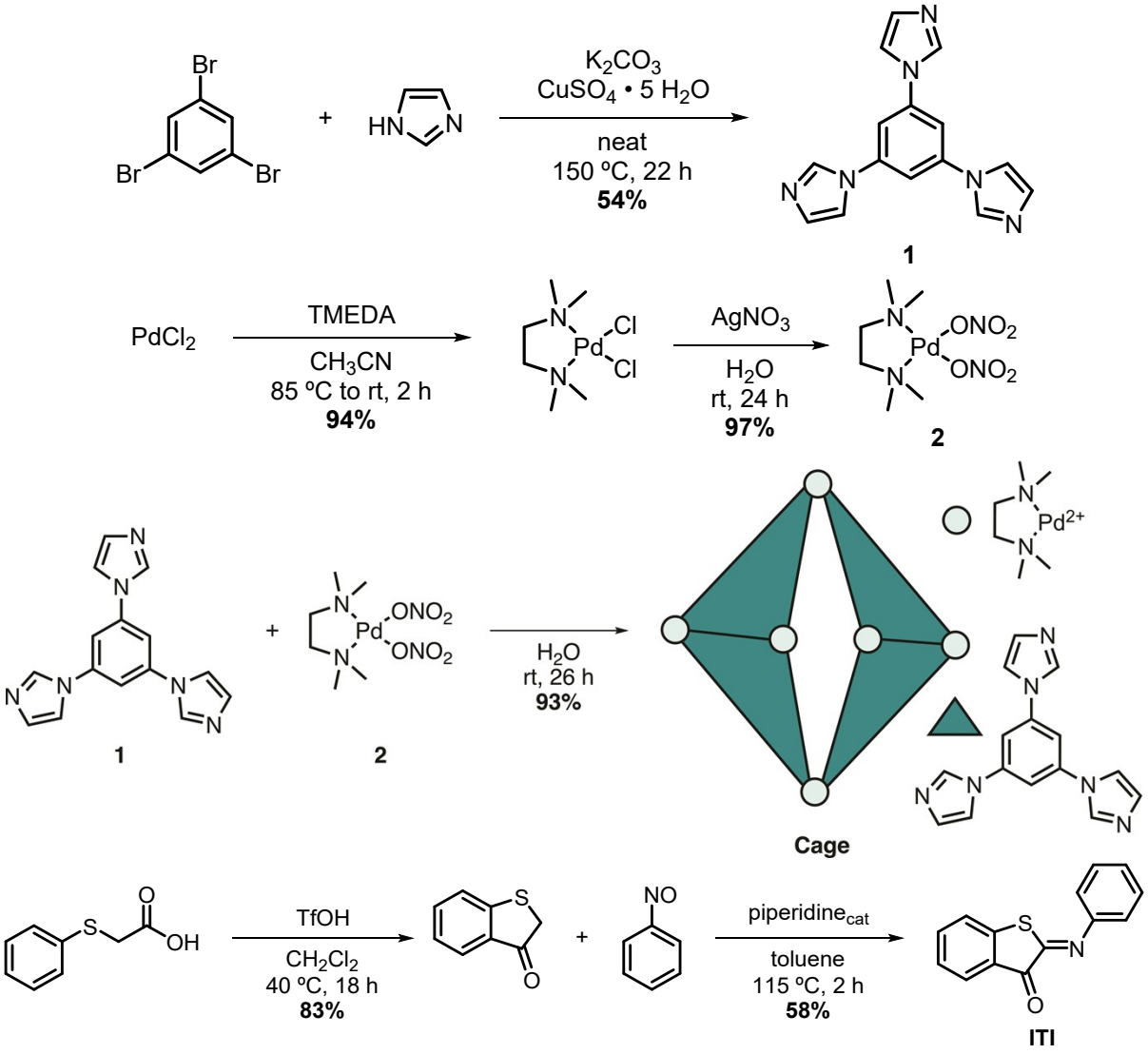

1,3,5-tri(1*H*-imidazol-1-yl)benzene (1)[1]

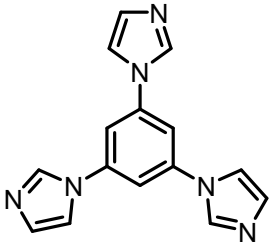

1
$C_{15}H_{12}N_6$
Mw: 276.30 g/mol

An oven-dried crimp top vial equipped with a stirring bar was charged with 1,3,5-tribromobenzene (1.52 g, 4.82 mmol, 1.0 eq.), K_2CO_3 (2.67 g, 19.3 mmol, 4.0 eq.), imidazole (1.95 g, 28.6 mmol, 5.9 eq.) and $CuSO_4 \cdot 5\ H_2O$ (31.1 mg, 0.13 mmol, 0.03 eq.). The vial was crimped, flushed with nitrogen and the mixture heated to 155 ºC for 22 h. The reaction mixture was allowed to cool down to room temperature, washed with water and filtered. The crude was concentrated under reduced pressure and recrystallized from MeOH to yield **1** as a colorless solid (722 mg, 2.61 mmol, 54%).

^{1}H NMR (600 MHz, $(CD_3)_2SO$)): δ = 8.54 (br s, 3H), 8.03 (br s, 3H), 7.96 (s, 3H), 7.18 (br s, 3H).
^{13}C{^{1}H} NMR (151 MHz, $(CD_3)_2SO$)): δ = 139.1, 136.1, 130.1, 118.3, 109.3.
HRMS-ESI (ESI+): calculated for $C_{15}H_{13}N_6$ $[M+H]^+$ 277.1196, found 277.1194.

Pd[TMEDA]Cl_2[2]

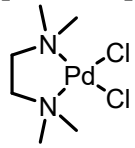

$C_6H_{16}Cl_2N_2Pd$
Mw: 293.53 g/mol

Under light exclusion, an oven-dried crimp top vial equipped with a stirring bar was charged with $PdCl_2$ (388 mg, 2.19 mmol, 1.0 eq.). The vial was crimped, flushed with nitrogen, dry CH_3CN (12.5 mL) added and the solution heated to 85 ºC for 2 h. The reaction mixture was allowed to cool down to room temperature, TMEDA (0.4 mL, 312 mg, 2.67 mmol, 1.2 eq.) was added and the mixture stirred for 30 min. The reaction mixture was then poured on Et_2O, filtered and dried to yield Pd[TMEDA]Cl_2 as yellow solid (602 mg, 2.05 mmol, 94%).

^{1}H NMR (600 MHz, $(CD_3)_2SO$)): δ = 2.72 (br s, 4H), 2.64 (s, 12H).
^{13}C{^{1}H} NMR (151 MHz, $(CD_3)_2SO$)): δ = 61.8, 50.5.
HRMS-ESI (ESI+): calculated for $C_6H_{15}N_2Pd$ [M-H-Cl_2]$^+$ 221.0265, found 221.0261.

Pd[TMEDA]$(NO_3)_2$ (2)[3]

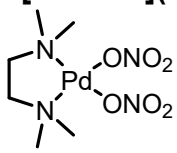

2
$C_6H_{16}N_4O_6Pd$
Mw: 346.64 g/mol

Under light exclusion, a crimp top vial equipped with a stirring bar was charged with Pd[TMEDA]Cl_2 (100 mg, 0.34 mmol, 1.0 eq.) suspended in deionized H_2O (5.5 mL). A solution of $AgNO_3$ (114.9 mg, 0.68 mmol, 2.0 eq.) in deionized H_2O (5.5 mL) was added dropwise. The vial was crimped, flushed with nitrogen and the mixture stirred at rt for 24 h. Remaining solids were filtered off *via* filtration over cotton wool, the solution extracted with $CHCl_3$ and the aqueous layer concentrated under reduced pressure to yield **2** as yellow solid (115 mg, 0.33 mmol, 98%).

^{1}H NMR (600 MHz, D_2O): δ = 2.89 (s, 4H), 2.69 (s, 12H).
^{13}C{^{1}H} NMR (151 MHz, D_2O): δ = 63.0, 50.2.
HRMS-ESI (ESI+): calculated for $C_6H_{15}N_2Pd$ [M-H-$(NO_3)_2$]$^+$ 221.0265, found 221.0265.

Cage[4]

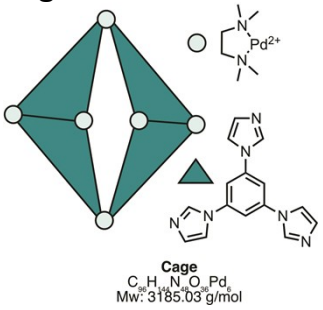

Under light exclusion, a crimp top vial equipped with a stirring bar was charged with **1** (61.0 mg, 0.33 mmol, 4.0 eq.) and a solution of **2** (115 mg, 0.22 mmol, 6.0 eq.) in deionized H_2O (14 mL) was added dropwise. The vial was crimped, flushed with nitrogen and the reaction mixture stirred at rt for 26 h. Remaining solids were filtered off *via* filtration over cotton wool, the obtained solution concentrated under reduced pressure and the solid washed with acetone to yield **Cage** as pale gray solid (65.9 mg, 0.05 mmol, 93%).

^{1}H NMR (600 MHz, D_2O): δ = 9.10 (s, 8H), 8.80 (s, 4H), 7.73 (s, 4H), 7.68 (s, 4H), 7.63 (s, 8H), 7.53 (s, 12H), 3.10 (s, 24H), 2.79 – 2.65 (m, 72H).
^{13}C{^{1}H} NMR (151 MHz, D_2O): δ = 138.0, 137.7, 137.4, 137.2, 128.7, 120.7, 120.5, 114.7 113.0, 62.5, 50.2, 50.2, 50.0.

Benzo[*b*]thiophen-3(2*H*)-one[5]

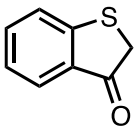

C_8H_6OS
Mw: 150.20 g/mol

An oven dried crimp top vial equipped with a stirring bar was charged with (phenylthiol)acetic acid (1.01 g, 5.98 mmol, 1.0 eq.). The vial was crimped, flushed with nitrogen and dry CH_2Cl_2 (12.0 mL) added. TfOH (2.7 mL, 4.58 g, 30.5 mmol, 5.1 eq.) was added dropwise and the reaction mixture heated to 40 ºC for 18 h. The reaction mixture was allowed to cool down to room temperature, poured onto an ice/water mixture, extracted with CH_2Cl_2 (3x) and the combined organic layers washed with aqueous $NaHCO_3$, dried over $MgSO_4$, the solvent removed under reduced pressure, yielding benzo[*b*]thiophen-3(2*H*)-one as brown solid (746 mg, 4.97 mmol, 83%), which was immediately further reacted.

^{1}H NMR (400 MHz, $CDCl_3$): δ = 7.78 (d, *J* = 7.8 Hz, 1H), 7.55 (t, *J* = 7.6 Hz, 1H), 7.43 (d, *J* = 8.0 Hz, 1H), 7.22 (t, *J* = 7.4 Hz, 1H), 3.80 (s, 2H).

Iminothioindoxyl (ITI)[6]

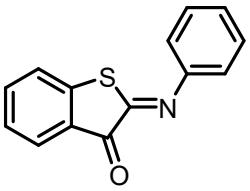

ITI
$C_{14}H_9NOS$
Mw: 239.29 g/mol

An oven dried crimp top vial equipped with a stirring bar was charged with benzo[*b*]thiophen-3(2*H*)-one (462 mg, 3.07 mmol, 1.0 eq.) and nitrosobenzene (528 mg, 4.93 mmol, 1.6 eq.). The vial was crimped, flushed with nitrogen, dry toluene (20 mL) and piperidine (40.0 μL) added and the reaction mixture heated under continuous stirring to 115 ºC for 2 h. The reaction mixture was allowed to cool down to room temperature, and extracted with CH_2Cl_2 and H_2O. The organic layer was washed with aqueous NH_4Cl, dried over $MgSO_4$, the solvent removed under reduced pressure and the crude product purified *via* flash column chromatography using a gradient starting from *n*-pentane to Et_2O yielding the **ITI** as an orange solid (426 mg, 1.78 mmol, 58%)

^{1}H NMR (600 MHz, $CDCl_3$): δ = 7.97 (dd, *J* = 7.7, 0.8 Hz, 1H), 7.62 (td, *J* = 7.6, 1.4 Hz, 1H), 7.49 – 7.44 (m, 2H), 7.41 (d, *J* = 7.9 Hz, 1H), 7.35 (td, *J* = 7.5, 1.0 Hz, 1H), 7.33 – 7.27 (m, 1H), 7.28 – 7.26 (m, 2H).
^{13}C{^{1}H} NMR (151 MHz, $CDCl_3$): δ = 185.6, 156.6, 149.7, 144.7, 137.1, 129.5, 128.0, 127.5, 126.9, 125.1, 121.2.
HRMS-ESI (ESI+): calculated for $C_{14}H_9NOSH^+$ $[M+H]^+$ 240.0478, found 240.0475.

NMR & UV-Vis Spectroscopy

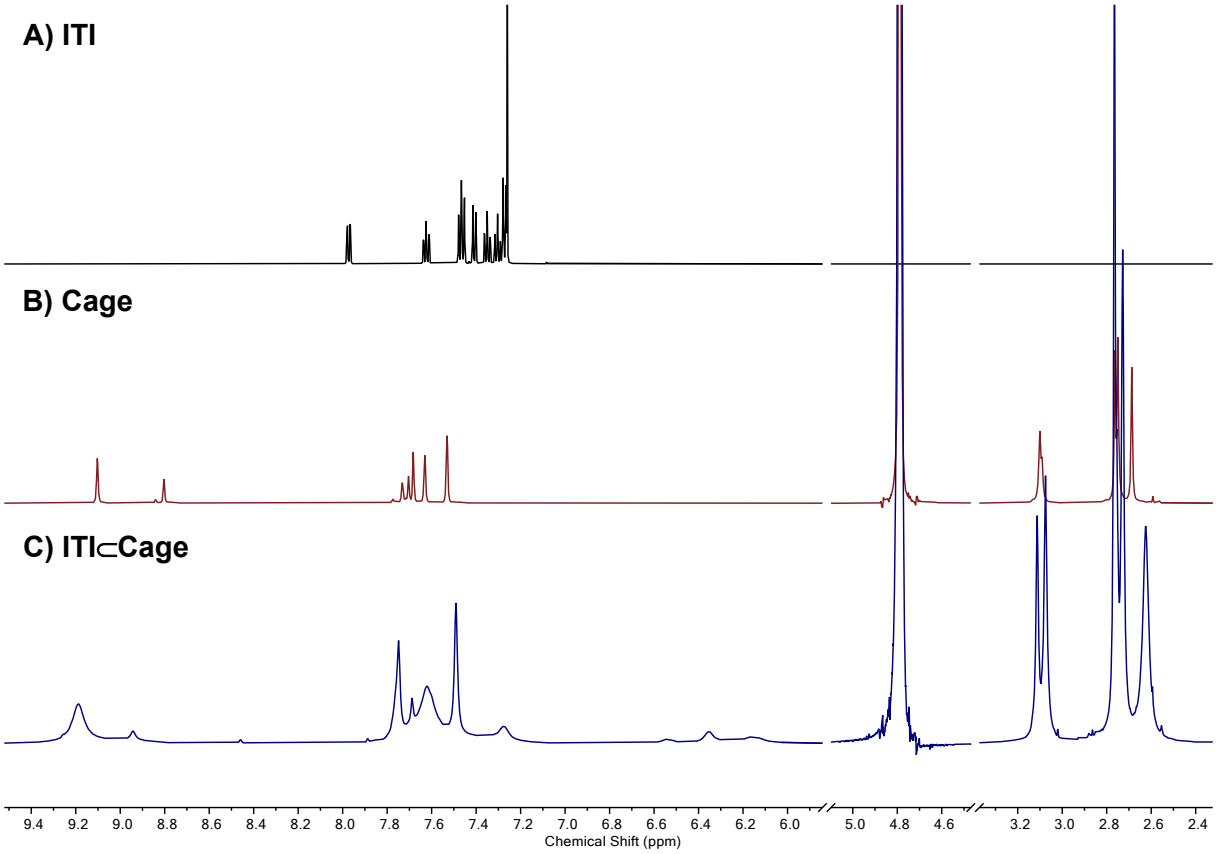

Figure S1: NMR spectra of **A) ITI** in $CDCl_3$, **B) Cage** in D_2O and **C) ITI⊂Cage** in D_2O (shift in signals and additional signals at δ = ~7.3 ppm and δ = 6.6 – 6.0 ppm).

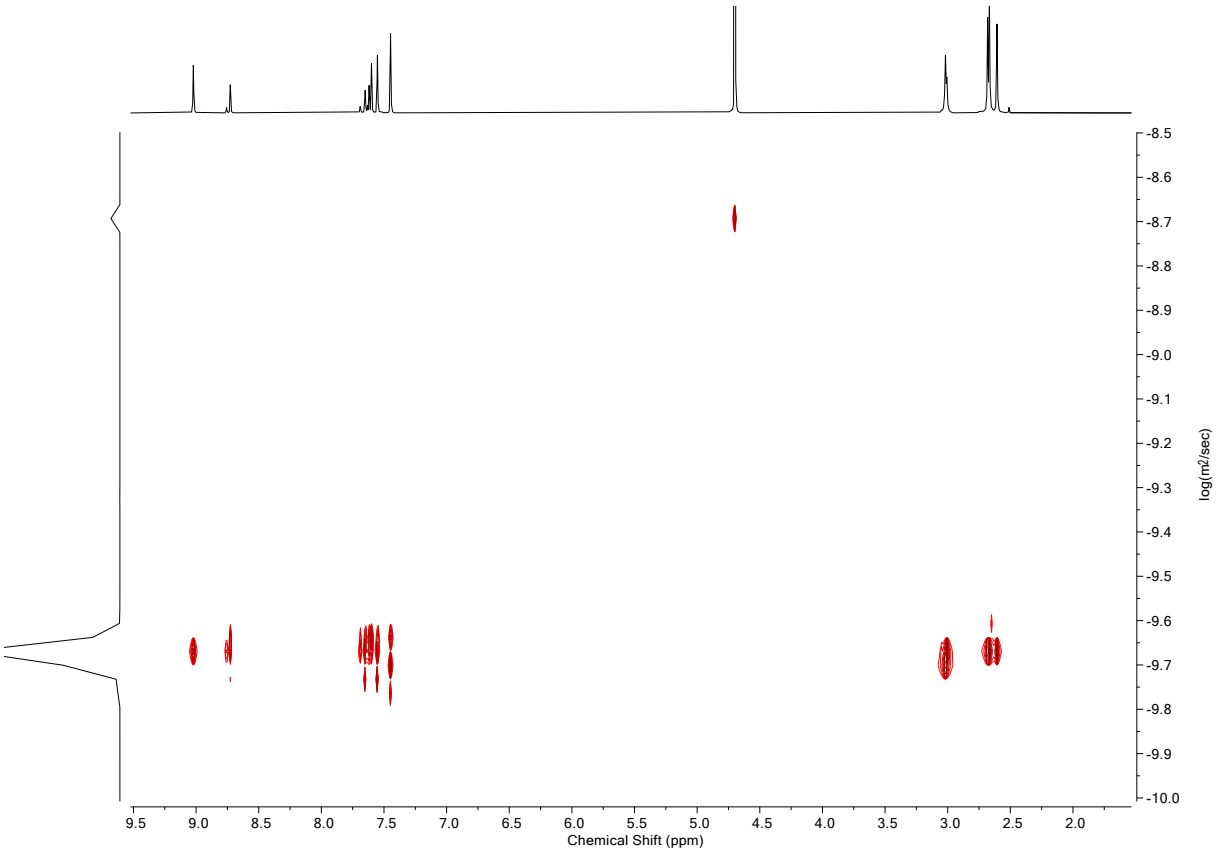

Figure S2: **^{1}H DOSY** spectrum of Cage (600 MHz, D_2O, 298 K, c = ~3 x 10^{-3} M).

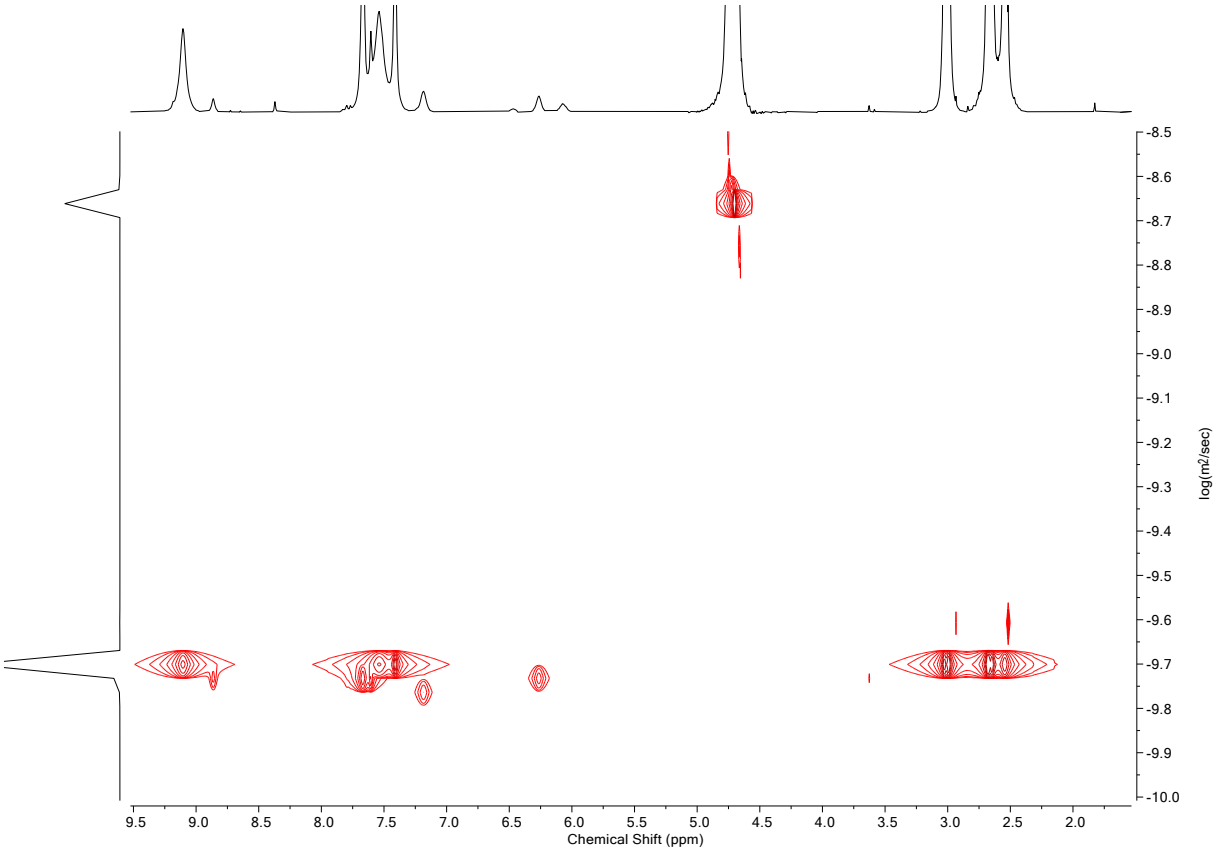

Figure S3: **^{1}H DOSY** spectrum of **ITI⊂Cage** (600 MHz, D_2O, 298 K, c = ~3 x 10^{-3} M).

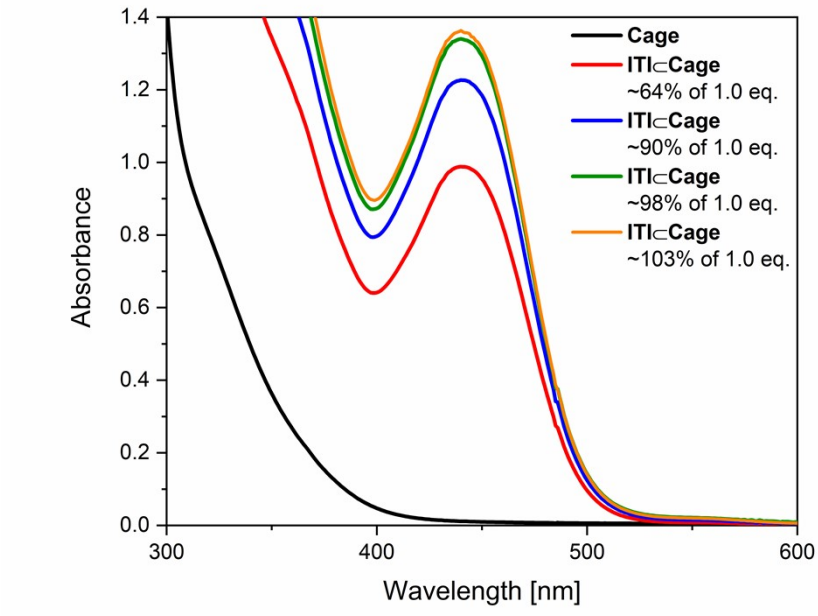

Figure S4: UV-Vis spectroscopy of weighted **ITI⊂Cage** solutions in D_2O (c = ~3 x 10^{-3} M) at 20 ºC. black = **Cage**; red = 64% of 1.0 eq. when 1.0 eq. were used; blue = 90% of 1.0 eq. when 2.0 eq. were used; green = 98% of 1.0 eq. when 3.0 eq. were used; orange = 103% of 1.0 eq. when 10.0 eq. were used.

Nanosecond Transient Absorption Spectroscopy

Nanosecond transient absorption spectra were recorded with an in-house assembled setup. To generate the excitation wavelength, a tunable Nd:YAG-laser system (NT342B, Ekspla) consisting of the pump laser (NL300) with harmonics generators (SHG, THG) producing 355 nm light to pump an optical parametric oscillator (OPO) with SHG connected into a single device was used. The laser system was operated with a pulse length of 5 ns and a repetition rate of 10 Hz. The probe light running at 20 Hz was generated by a high-stability short arc xenon flash lamp (FX-1160, Excelitas Technologies) employing a modified PS302 controller (EG&G). The probe light was split equally into a signal and a reference beam by means of a 50/50 beam splitter and focused (bi-convex lens 75 mm) on the entrance slit of a spectrograph (SpectraPro-150, Princeton Instruments) with a grating of 150 ln mm^{-1}, blaze at 500 nm. The probe beam (A = 1 mm^2) was set to pass through the sample cell and orthogonally overlapped with the excitation beam on a 1 mm × 1 cm area. The excitation energy was determined by recording the excitation power at the back of an empty sample holder. To correct for fluctuations in the spectral intensity of the flash lamp, the signal was normalized using the reference. The two beams were recorded at the same time using a gated intensified CCD camera (PI-MAX3, Princeton Instruments) with an adjustable gate of minimal 2.9 ns. Under standard settings, a gate of 20 ns and software binning were used to improve the dynamic range and signal to noise ratio. Two delay generators (DG535 and DG645, Stanford Research Systems, Inc.) were used to trigger the excitation and to change the delay of the flash lamp together with the gate of the camera during the experiment. An in-house Labview program was used to control the setup. The data was analyzed by means of singular value decomposition and global analysis, employing the software Glotaran 1.5.1.[8]

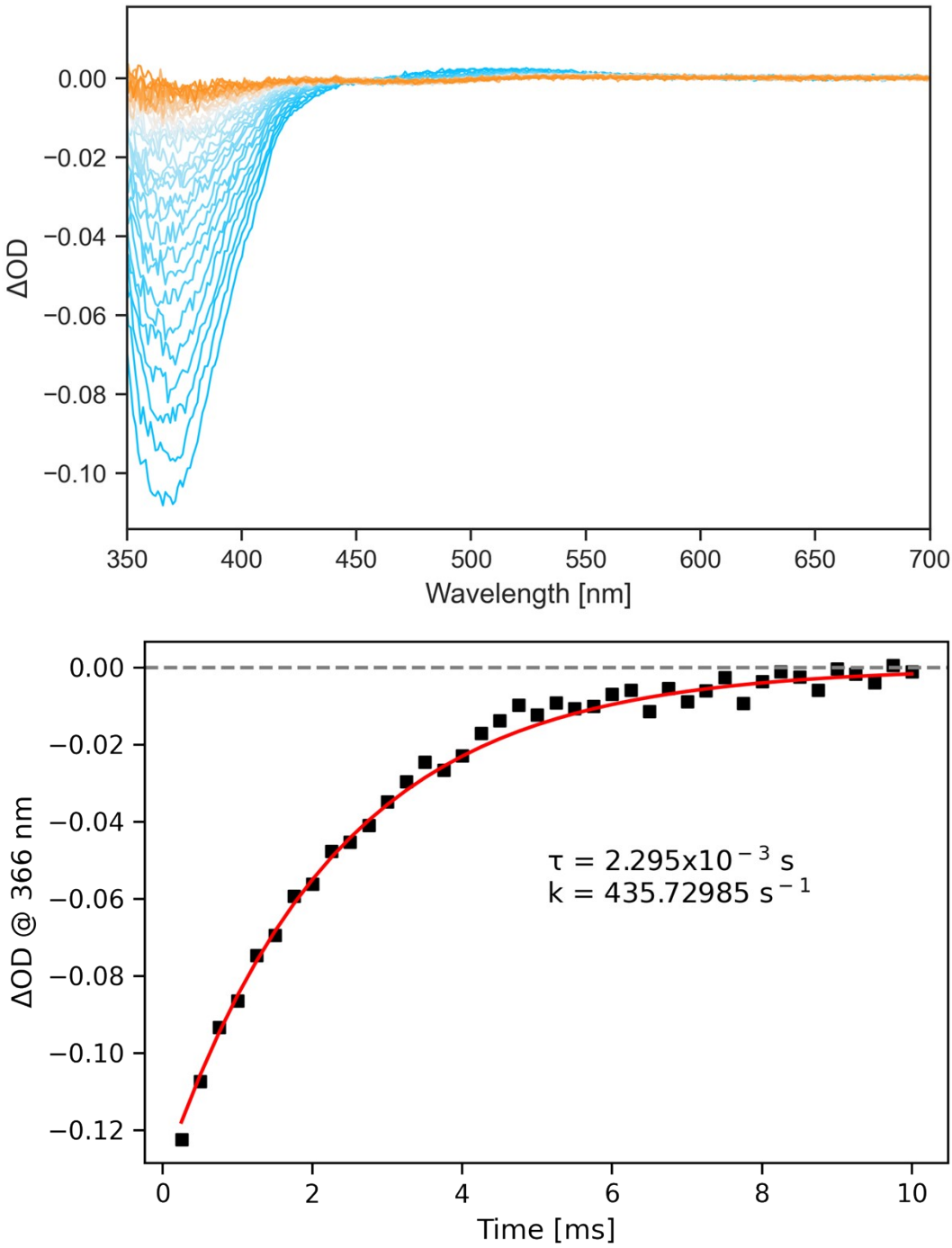

Figure S5: Nanosecond transient absorption of **ITI⊂Cage** in D_2O at room temperature. The sample was irradiated at 430 nm (1.06 OD, 1.6 mJ) upon which the spectrum was recorded in steps of increasing delay. Bottom: Fit of the decay of the absorption maximum of the transient signal (red line) as obtained from a global analysis of the transient absorption spectra in the top panel.

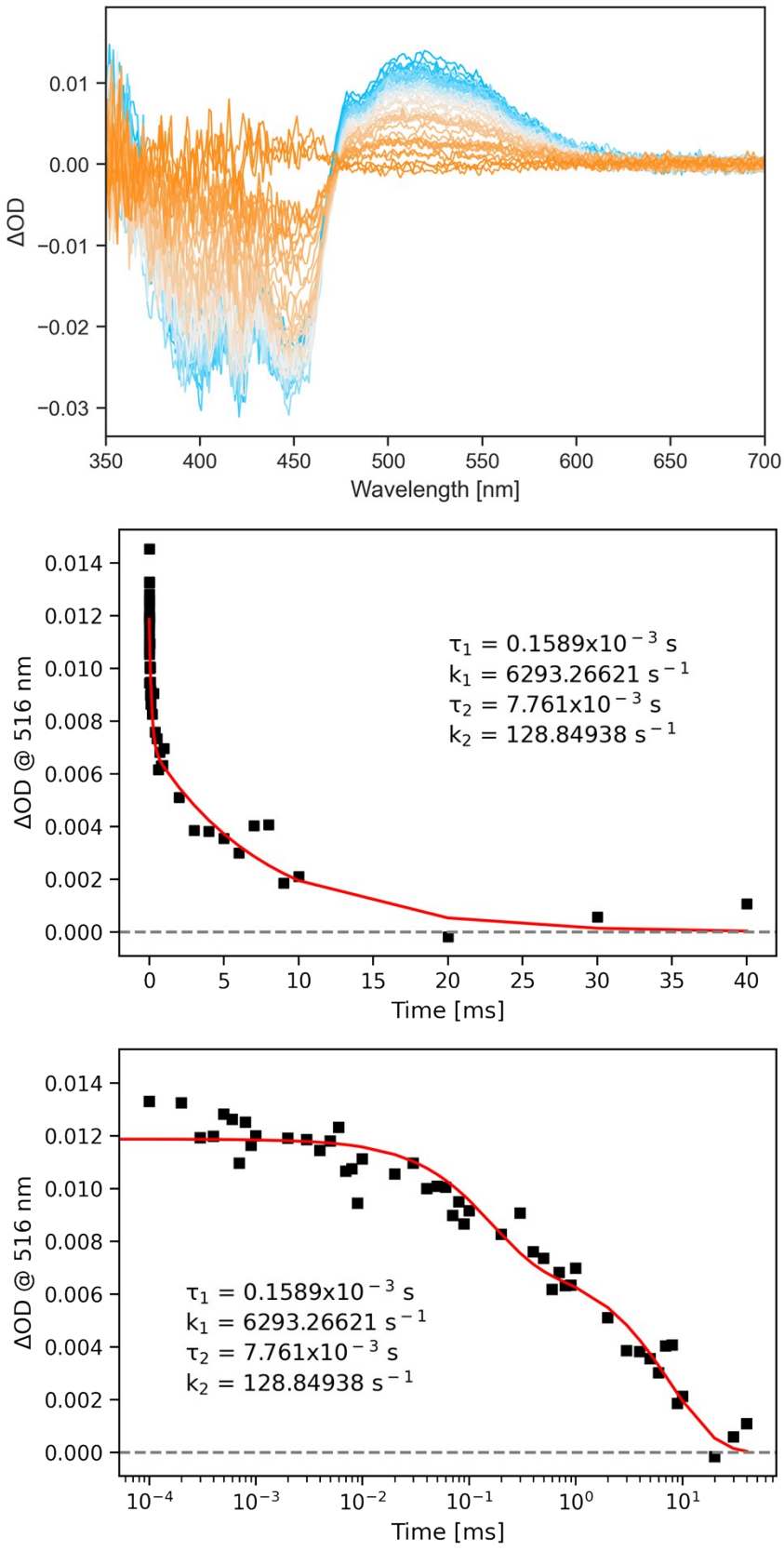

Figure S6: Nanosecond transient absorption of **ITI** in a thin PMMA film at room temperature. The sample was irradiated at 430 nm (1 mJ) upon which the spectrum was recorded in steps of increasing delay. Center: Fit of the decay of the absorption maximum of the transient signal (red line) as obtained from a global analysis of the transient absorption spectra in the top panel. Bottom: LinLog plot of the fit reported in the central panel.

Femtosecond Transient Absorption Spectroscopy

The apparatus used for the transient absorption spectroscopy (TAS) measurements has been described in detail before.[6] Briefly, 80 fs pulses centered at 810 nm were produced by an integrated home-made Ti:sapphire oscillator coupled with a regenerative amplifier system (Amplitude Pulsar). The excitation wavelength was set at 400 nm, obtained as the second harmonic of the fundamental laser radiation, and excitation power was set at 30-50 nJ for all measurements. The pump beam polarization has been set to the magic angle with respect to the probe beam by rotating a λ\2 plate, to exclude rotational contributions. The white light probe pulse was generated by focusing a small portion of the fundamental laser radiation on a 3 mm thick CaF_2 window. A portion of the generated white light was sent to the sample through a different path and used as a reference signal. After passing through the sample the white light probe and reference pulses were both directed to a flat field monochromator coupled to a home-made CCD detector. Transient signals were acquired in a time interval spanning up to 500 ps. The sample was contained in a 2 mm quartz cuvette, mounted on a movable holder in order to minimize photodegradation. Measurements were performed at room temperature. Concentrations were adjusted to an absorbance of 0.9 – 1.0 OD (for the respective optical path) at the absorption maximum, which amounted to about 0.3 – 0.5 OD at the excitation wavelength (**ITI⊂Cage** solutions in D_2O; c = ~3 x 10^{-3} M). Before and after the measurements, the integrity of the sample was checked on a PerkinElmer LAMBDA 950 spectrophotometer. The data was analyzed by means of singular value decomposition, global and transient analysis, employing the software Glotaran 1.5.1.[8]

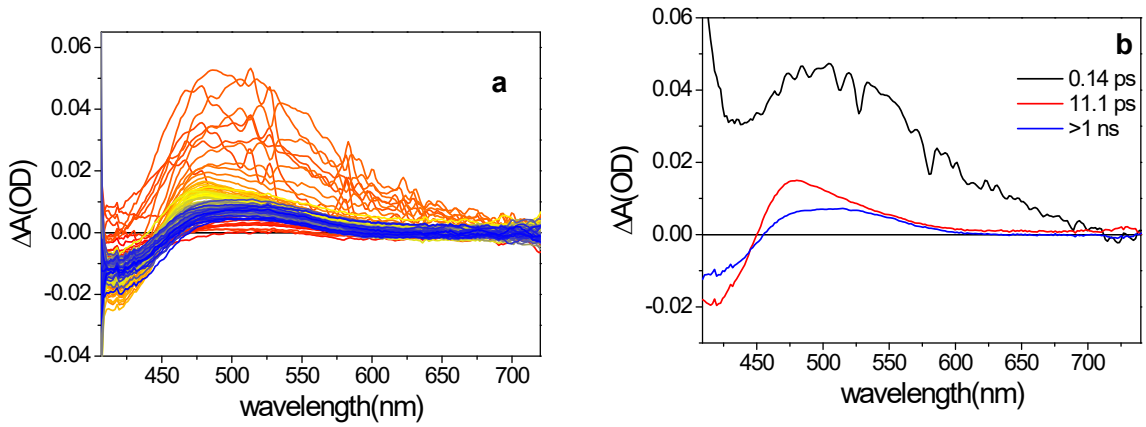

Figure S7: Transient absorption spectra (left) and EADS (right) obtained from global analysis of the kinetic traces registered for **ITI** dispersed in PMMA upon excitation at 400 nm.

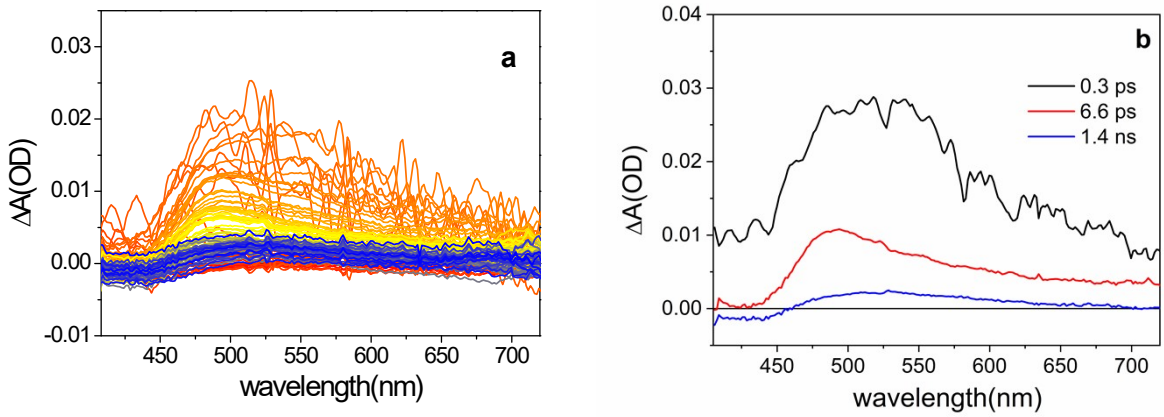

Figure S8: Transient absorption spectra (left) and EADS (right) obtained from global analysis of the kinetic traces registered for **ITI** dispersed in the molecular **Cage** in D_2O upon excitation at 400 nm.

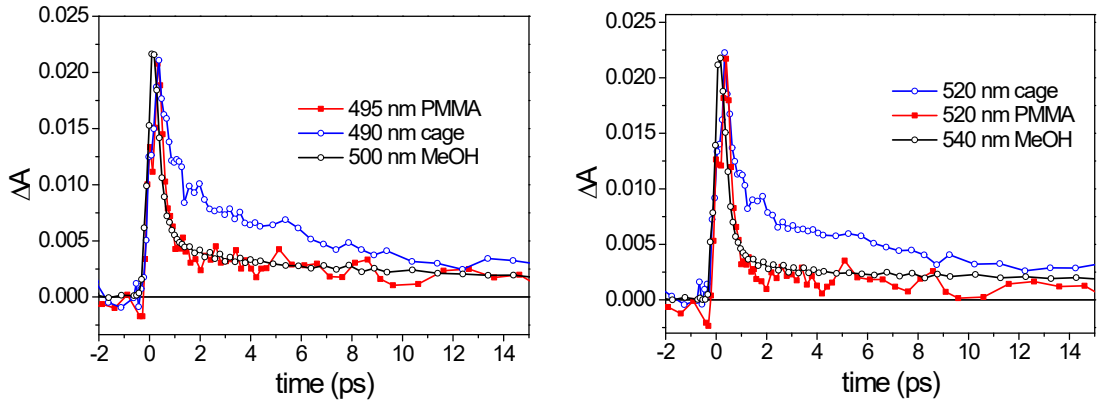

Figure S9: Comparison of selected kinetic traces measured for **ITI** in methanol, PMMA and **Cage**.

Molecular Dynamics Simulations

Five different conformations were obtained by placing one **ITI** in a Pd-metal-organic **Cage**. These structures were optimized using the semiempirical tight binding software xTB 6.6.1[9] at the GFN-FF[10] level together with the GBSA solvation model.[11] The CREST[12] utility of xTB 6.4.0[9] with GFN-FF[10] in combination with the GBSA solvation model[11] and the Quantum Cluster Growth (QCG) algorithm[13] was used for the addition of explicit 500 water molecules. QCG uses two different wall potentials to construct the solvated environment, namely a first one around the solute, which fixes it to prevent it from drifting when constructing the solvent shell, and a second one around the entire system. The molecular dynamic simulations (MD) were carried out on each structure with xTB 6.5.0[9] on GFN-FF[10] level after removing the internal wall potential used to build the solute-solvent system. The simulation was run for 5000 ps with 2.0 fs time intervals. The bonds were constrained from breaking using the SHAKE algorithm and the hydrogen mass was set at 4 au to increase the stability of the run. The temperature was set at 298.15 K and maintained with a Berendsen thermostat. A selection of 1000 structures was randomly chosen for further inspection. The selection was made using the mdsample.py tool from the MNDO2020 software package.[14]

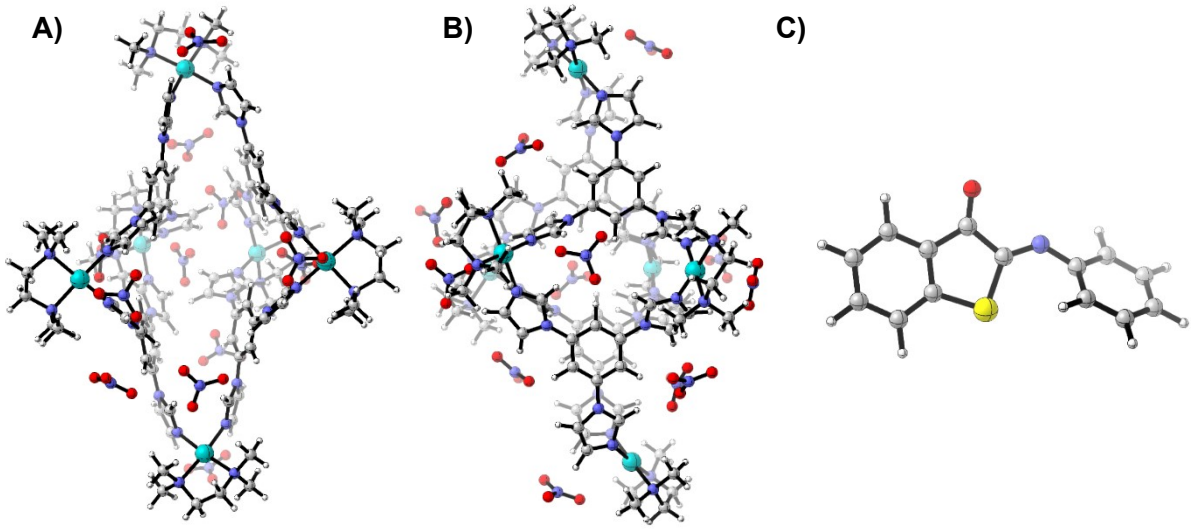

Figure S10: Pd-metal-organic cage **A)** front view, **B)** side view, **C) ITI** switch.

To define the system of the cage combined with one **ITI**, the orientation of the phenyl ring of the **ITI** and the **ITI** itself was considered. **Table S1** defines the orientation of the **ITI** inside and outside of the **Cage**.

Table S1: Description of the orientation of the **ITI** inside and outside the Pd-metal-organic **Cage**.

a	**ITI** is vertically orientated and incorporated in the **Cage**
b	**ITI** is horizontally orientated and incorporated in the **Cage**; the phenyl ring is inside the **Cage**
c	**ITI** is horizontally orientated and incorporated in the **Cage**; the phenyl ring is outside the **Cage**
d	**ITI** is outside and in front of the **Cage**
e	**ITI** is outside and on the side of the **Cage**

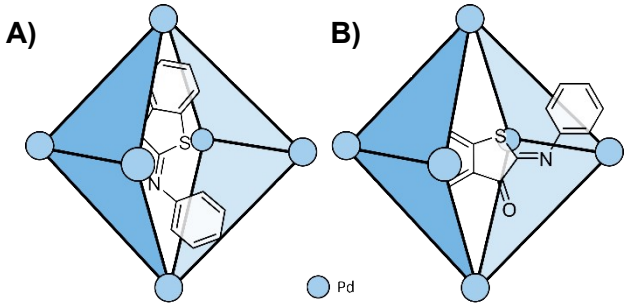

Figure S11: Orientation of one **ITI** inside the Pd-metal-organic **Cage**. **A) ITI** is vertically orientated and incorporated into the **Cage**. **B) ITI** is horizontally orientated and incorporated into the **Cage**, with the phenyl ring pointing outside the **Cage**.

The energy difference between the various orientations and positions of the **ITI** combined with the **Cage** was evaluated using 1000 randomly selected structures obtained from the MD, as shown in **Figure S10**.

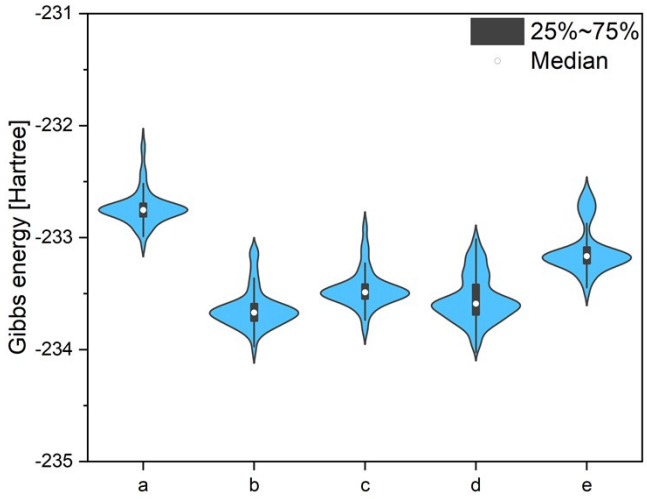

Figure S12: Gibbs free energy [Hartree] distribution of the Pd-metal-organic **Cage** in combination with one **ITI** from 1000 samples of the MD simulation. **a**: **ITI** is vertically orientated and incorporated in the **Cage**. **b**: **ITI** is horizontally orientated and incorporated in the **Cage** with the phenyl ring inside the **Cage**. **c**: **ITI** is horizontally orientated and incorporated in the **Cage** with the phenyl ring outside the **Cage**. **d**: **ITI** is in front of the **Cage**. **e**: **ITI** is on the side of the **Cage**.

Table S2 shows the Median of each data set for the systems **a-e**.

Table S2: Median of the Gibbs energy from the systems **a-e** corresponding to **Figure S8**.

System	Median [Hartree]
a	-232.735
b	-233.640
c	-233.465
d	-233.549
e	-233.111

Figure S10 and **Table S2** show that the structure with the highest median energy was obtained with **a** and the lowest with **b**. The energy difference was explained by the difference in the **Cage** structure between the two systems. The **Cage** of **a** opened up and formed a pocket to incorporate the **ITI** molecule, as shown in **Figure S11 A)**. On the other hand, the structure of the **Cage** in **b** (see **Figure S11 B)**) was more closed and compact, similar to the structure of the single **Cage** (**Figure S8**). The slightly less stable structure **c** was obtained with the phenyl ring of the **ITI** switch outside of the **Cage**. However, **Figure S11 C)** showed that the degree of deformation of the **Cage** in **c** is similar to that in **b**. Placing **ITI** outside the **Cage** has in both cases a destabilizing effect and is therefore higher in energy than **b**.

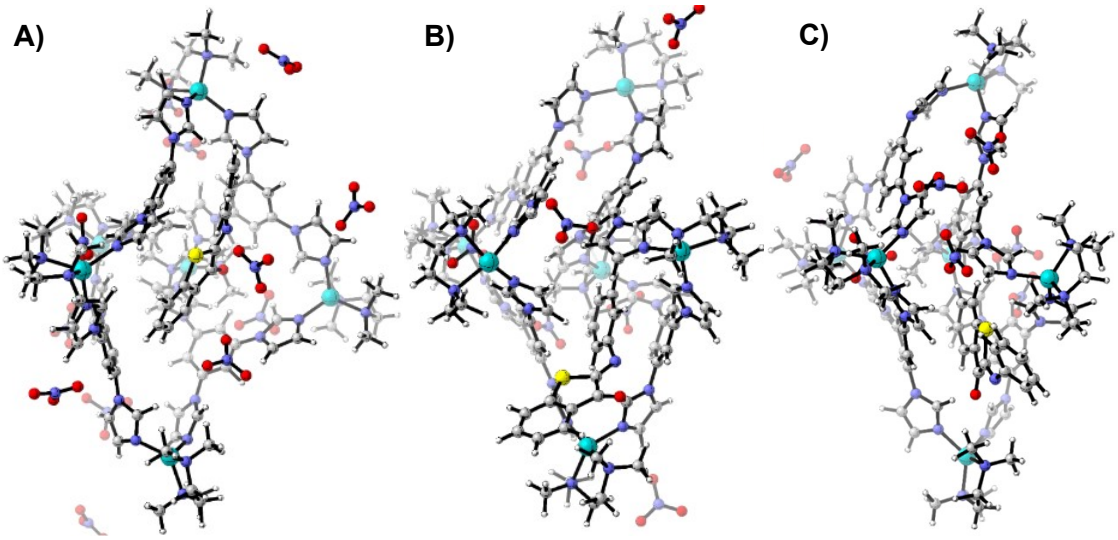

Figure S13: Excerpt from system **A) a**: vertically oriented and incorporated in **Cage**, **B) b**: horizontally oriented and the phenyl ring inside the **Cage** and **C) c:** horizontally oriented and the phenyl ring outside the **Cage**; without water molecules from QCG; structure sample from MD simulation.

References

1 A. Rit, T. Pape and F. E. Hahn, J. Am. Chem. Soc., 2010, 132, 4572–4573.
2 R. P. King and S. L. Buchwald, Organometallics, 2019, 38, 3490–3493.
3 S. H. A. M. Leenders, R. Becker, T. Kumpulainen, B. de Bruin, T. Sawada, T. Kato, M. Fujita and J. N. H. Reek, Chem. Eur. J., 2016, 22, 15468–15474.
4 D. Samanta, D. Galaktionova, J. Gemen, L. J. W. Shimon, Y. Diskin-Posner, L. Avram, P. Král and R. Klajn, Nat. Commun., 2018, 9, 641.
5 A. Gernet, A. El Rhaz and L. Jean, Chem. Eur. J., 2023, 29, e202301160.
6 M. W. H. Hoorens, M. Medved', A. D. Laurent, M. Di Donato, S. Fanetti, L. Slappendel, M. Hilbers, B. L. Feringa, W. Jan Buma and W. Szymanski, Nat. Commun., 2019, 10, 2390.
7 K. Hema, A. B. Grommet, M. J. Białek, J. Wang, L. Schneider, C. Drechsler, O. Yanshyna, Y. Diskin-Posner, G. H. Clever and R. Klajn, J. Am. Chem. Soc., 2023, 145, 24755–24764.
8 J. J. Snellenburg, S. P. Laptenok, R. Seger, K. M. Mullen and I. H. M. Van Stokkum, J. Stat. Softw., 2012, 49, 1–22.
9 C. Bannwarth, E. Caldeweyher, S. Ehlert, A. Hansen, P. Pracht, J. Seibert, S. Spicher and S. Grimme, Wiley Interdiscip. Rev. Comput. Mol. Sci., 2021, 11, e1493.
10 S. Spicher and S. Grimme, Angew. Chem. Int. Ed., 2020, 59, 15665–15673.
11 S. Ehlert, M. Stahn, S. Spicher and S. Grimme, J. Chem. Theory Comput., 2021, 17, 4250–4261.
12 P. Pracht, F. Bohle and S. Grimme, Phys. Chem. Chem. Phys., 2020, 22, 7169–7192.
13 S. Spicher, C. Plett, P. Pracht, A. Hansen and S. Grimme, J. Chem.Theory Comput., 2022, 18, 3174–3189.
14 W. Thiel, MNDO2020: A Semiempirical Quantum Chemistry Program 2020.

Appendix

NMR Spectra

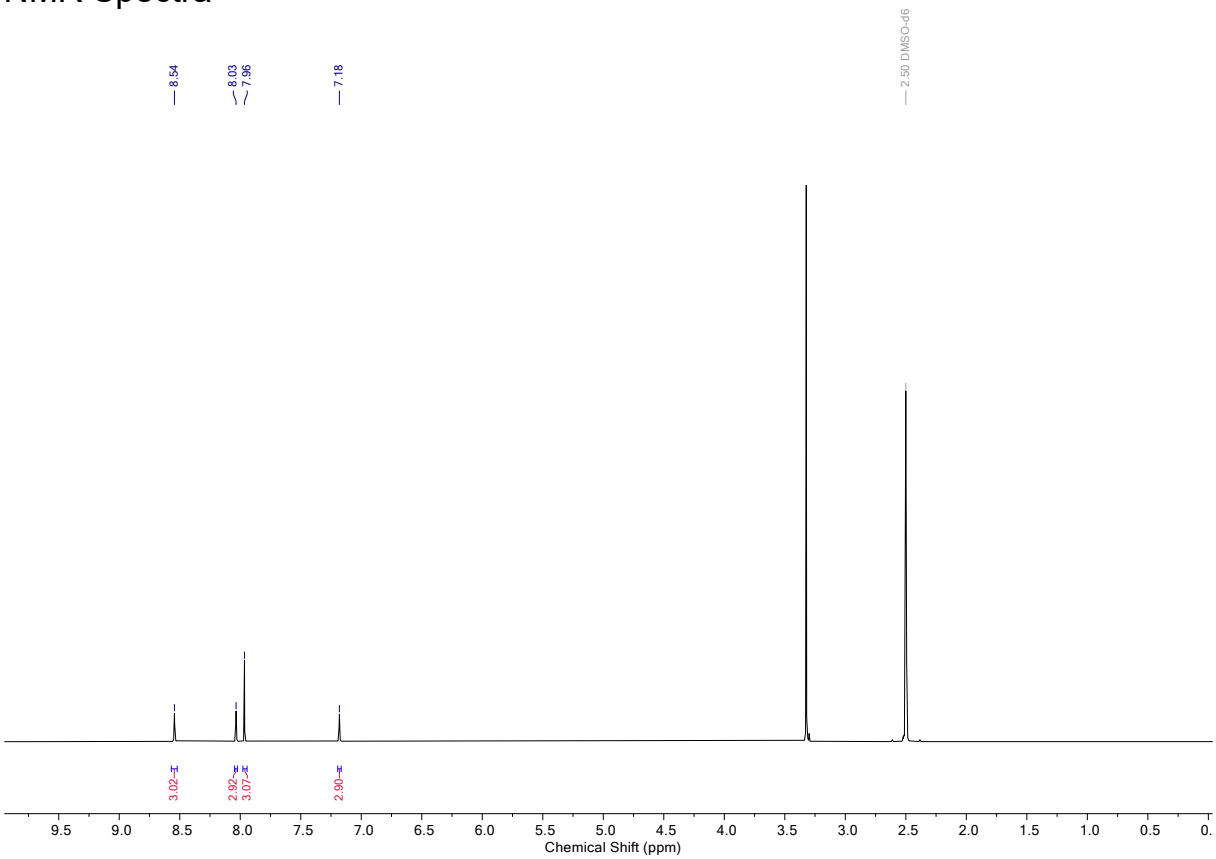

Figure S14: ^{1}H NMR spectrum of **1** ($(CD_3)_2SO$).

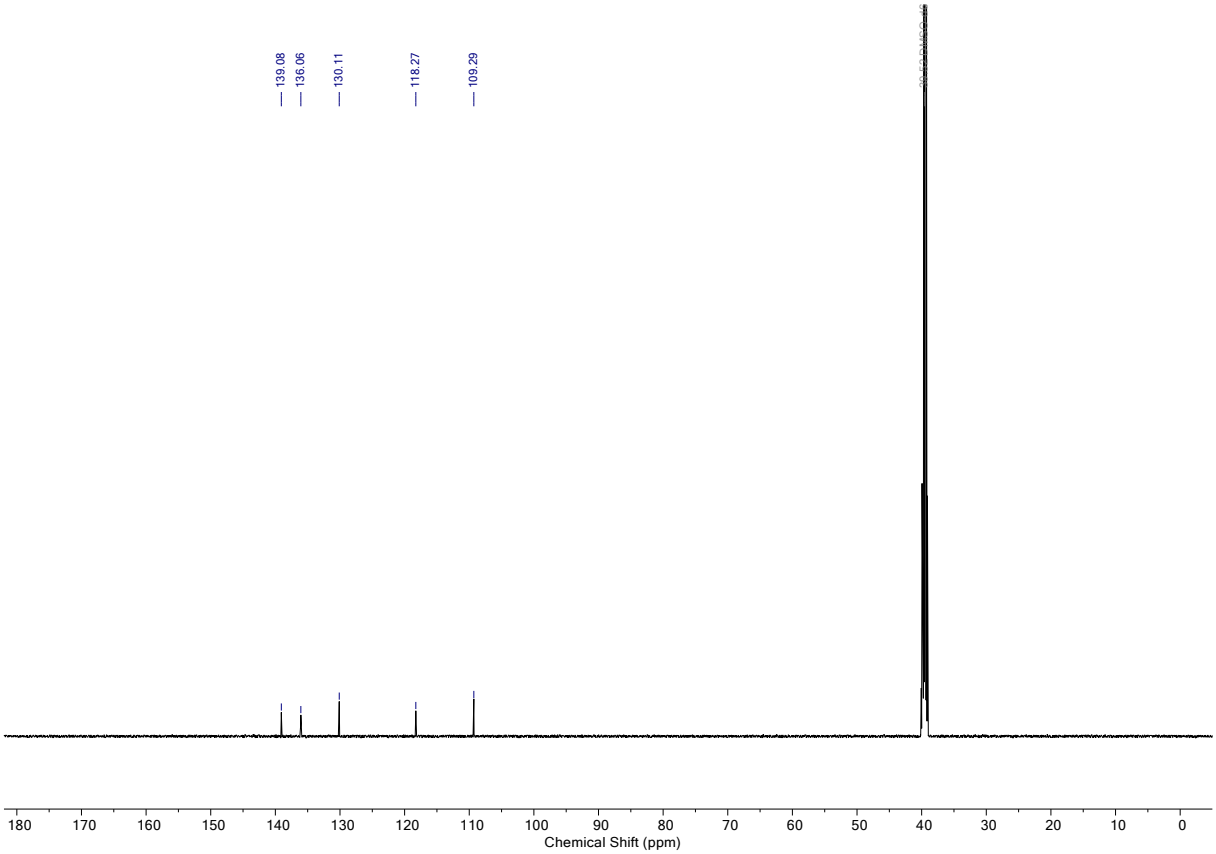

Figure S15: ^{13}C{^{1}H} NMR spectrum of **1** ($(CD_3)_2SO$).

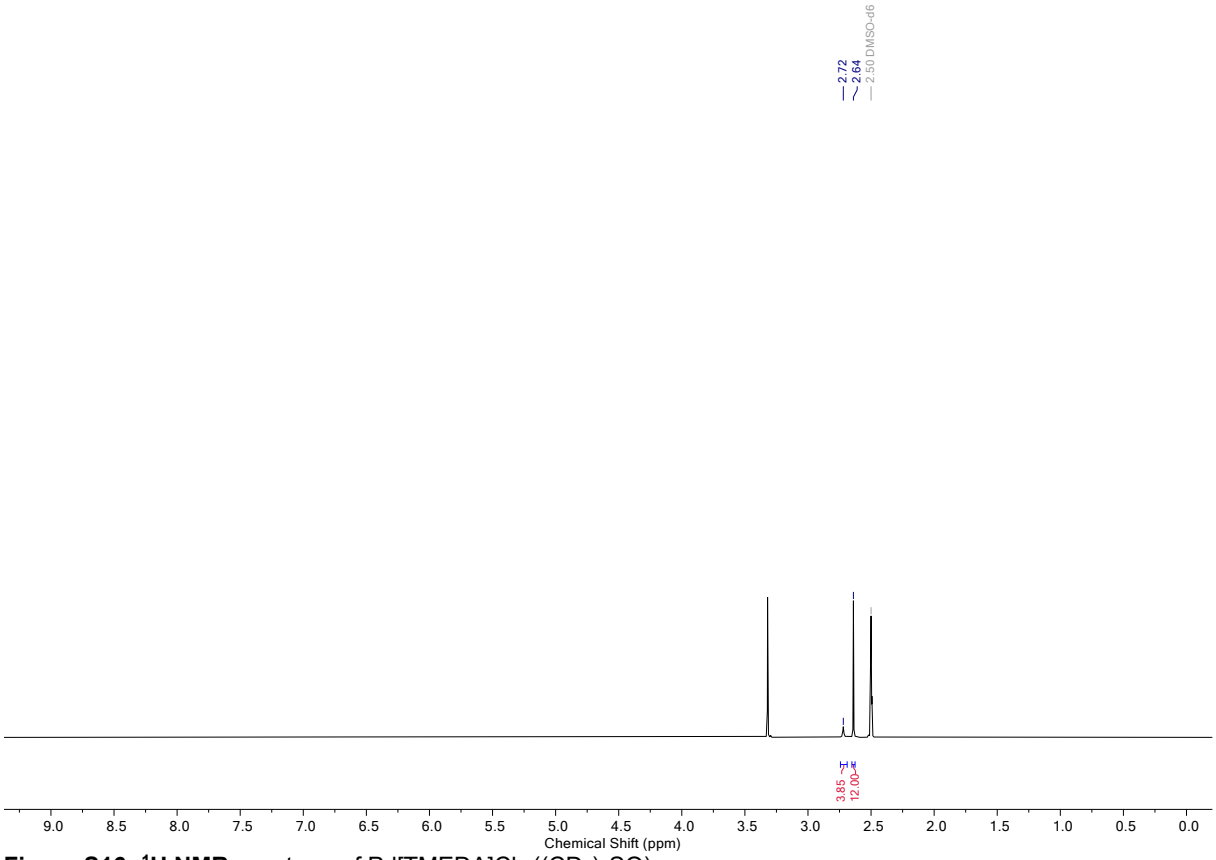

Figure S16: ^{1}H NMR spectrum of Pd[TMEDA]Cl_2 ($(CD_3)_2SO$).

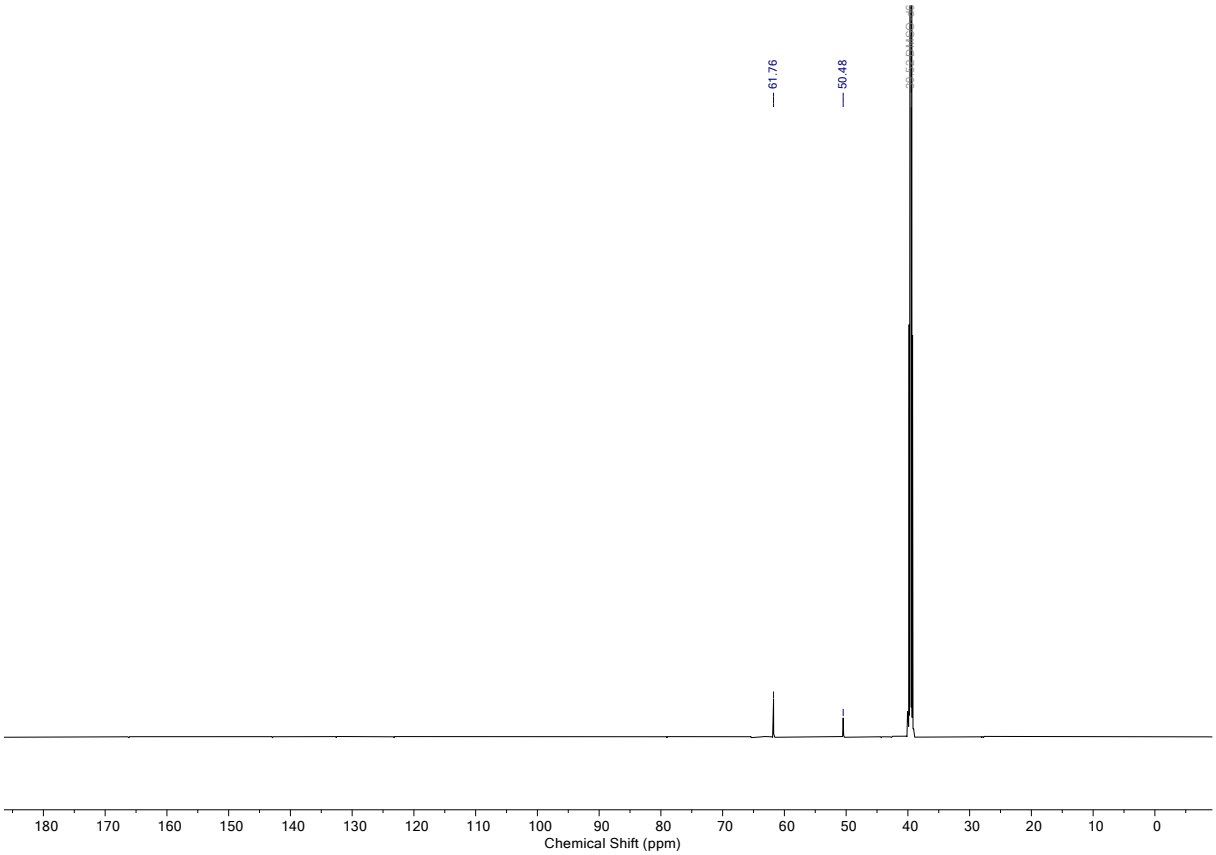

Figure S17: ^{13}C{^{1}H} NMR spectrum of Pd[TMEDA]Cl_2 ($(CD_3)_2SO$).

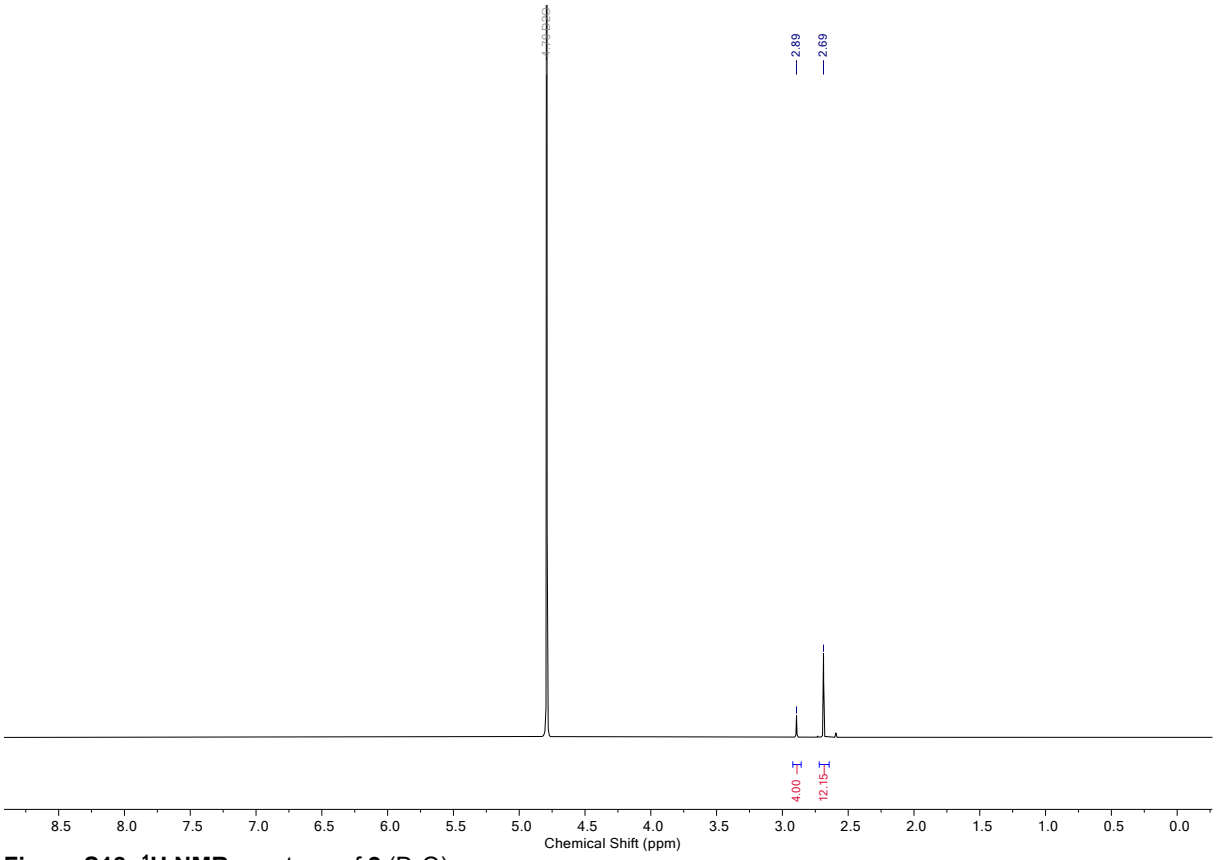

Figure S18: ^{1}H NMR spectrum of **2** (D_2O).

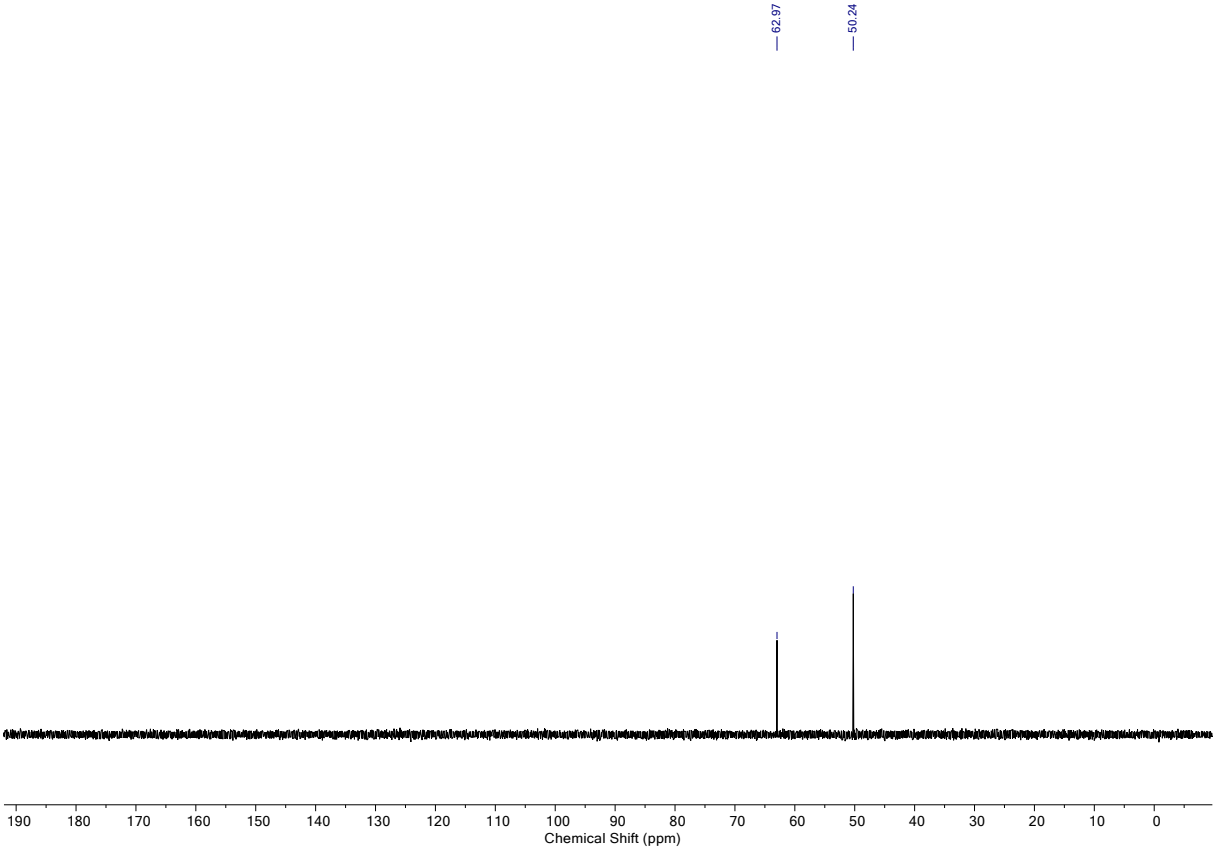

Figure S19: ^{13}C{^{1}H} NMR spectrum of **2** (D_2O).

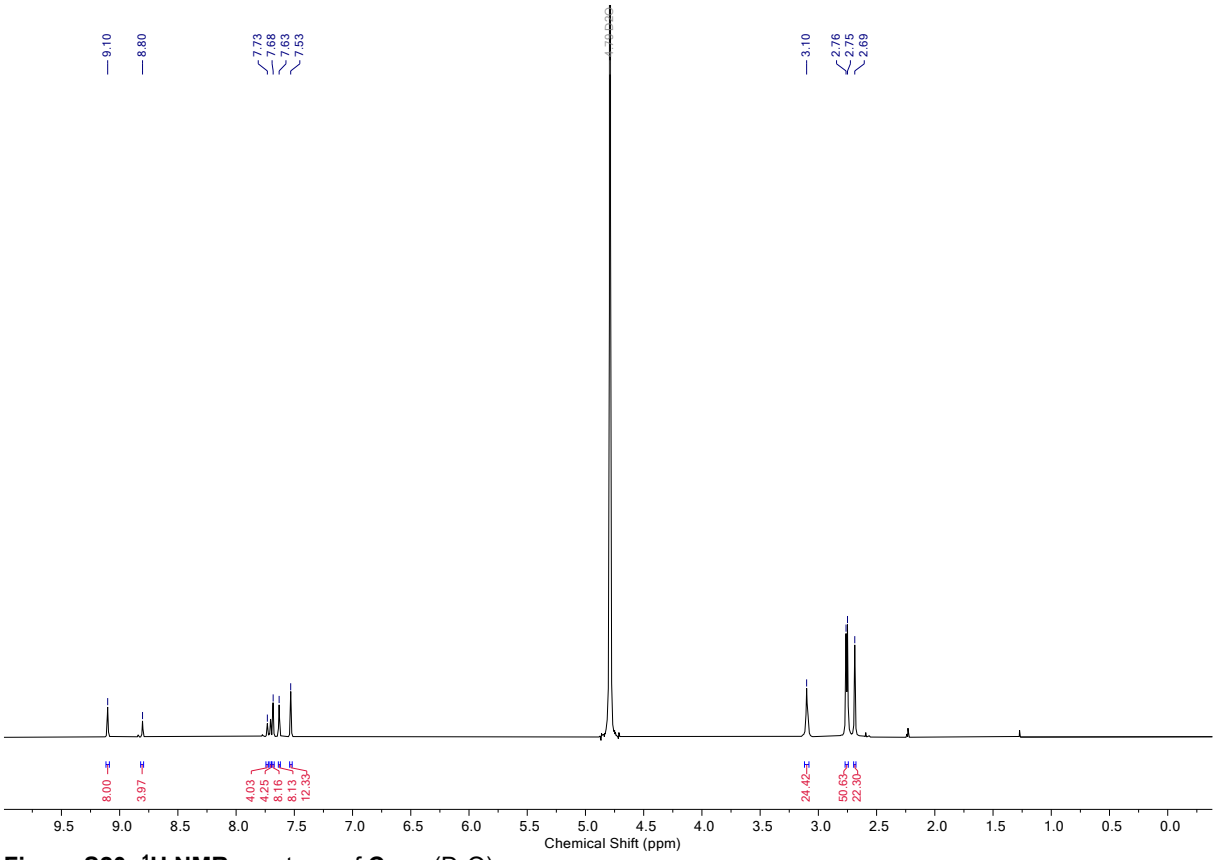

Figure S20: ^{1}H NMR spectrum of **Cage** (D_2O).

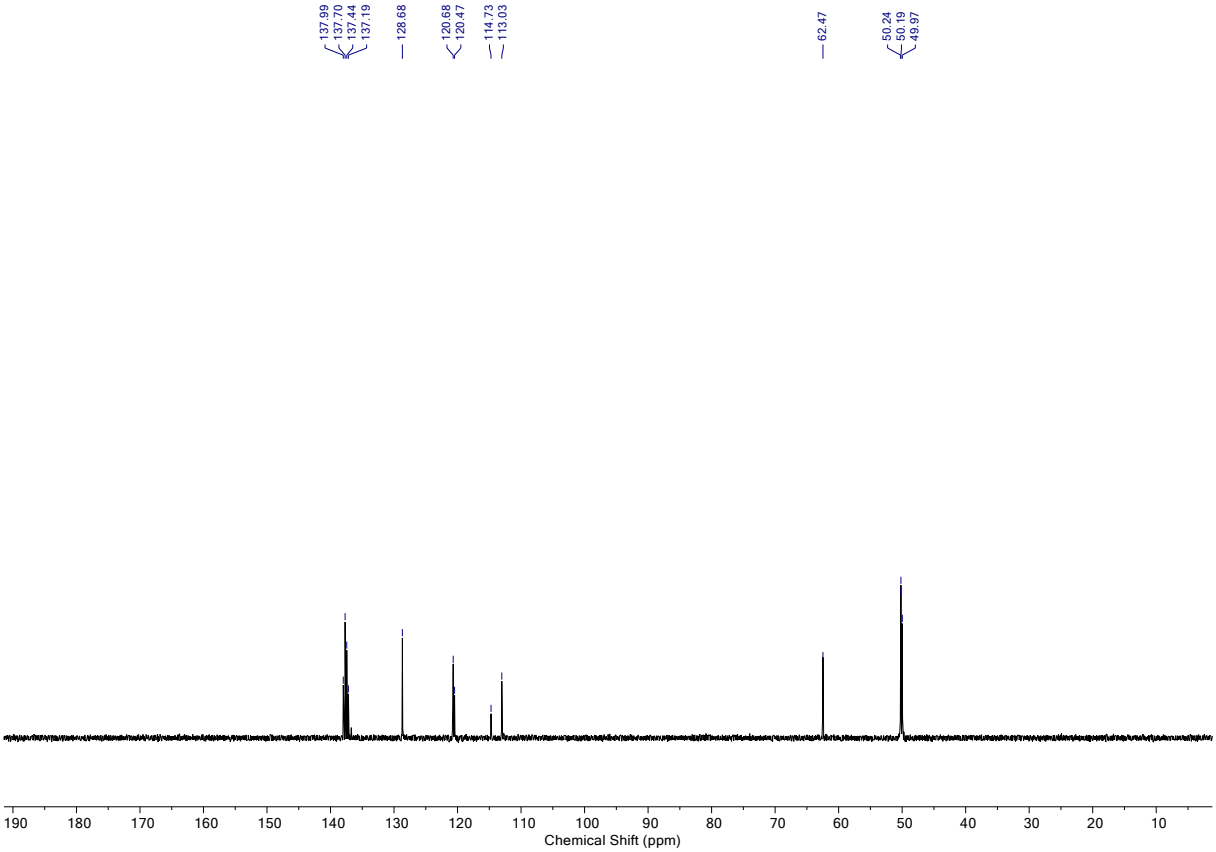

Figure S21: ^{13}C{^{1}H} NMR spectrum of **Cage** (D_2O).

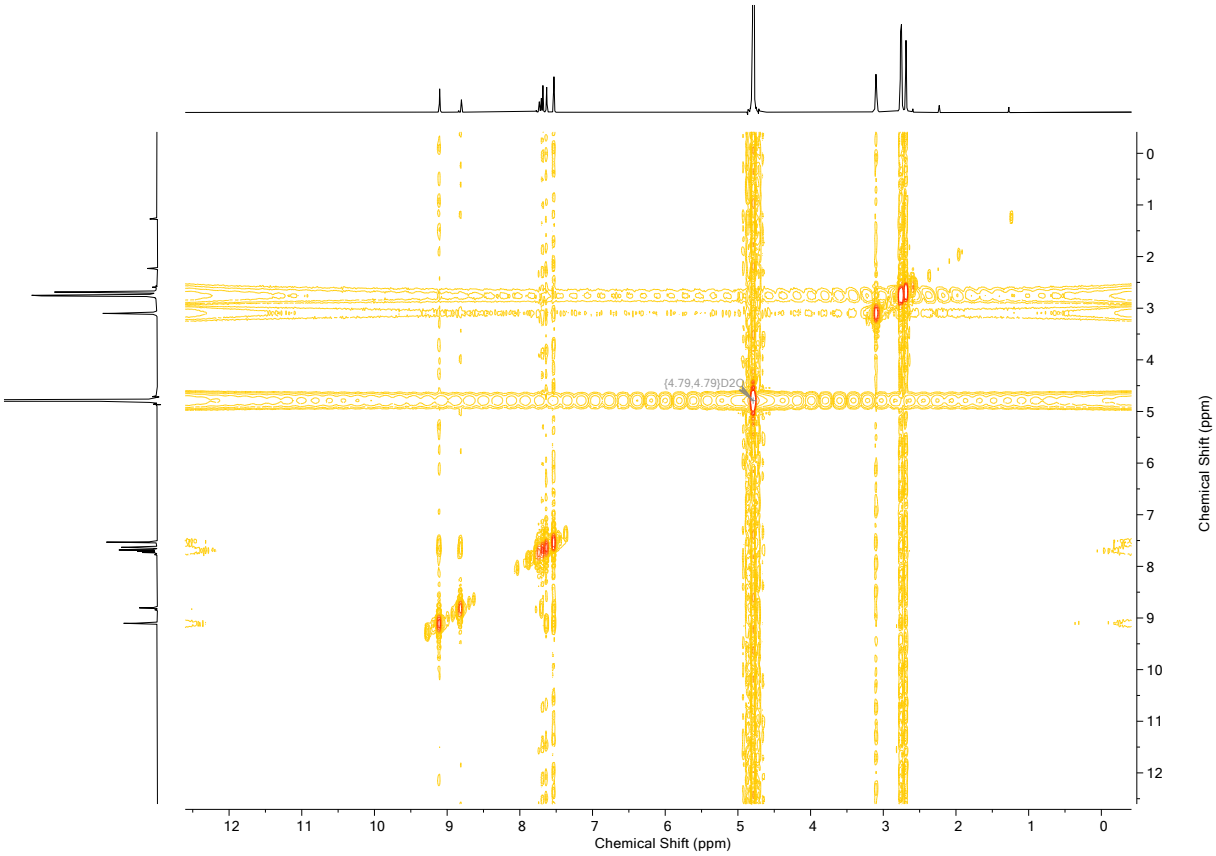

Figure S22: COSY spectrum of **Cage** (D_2O).

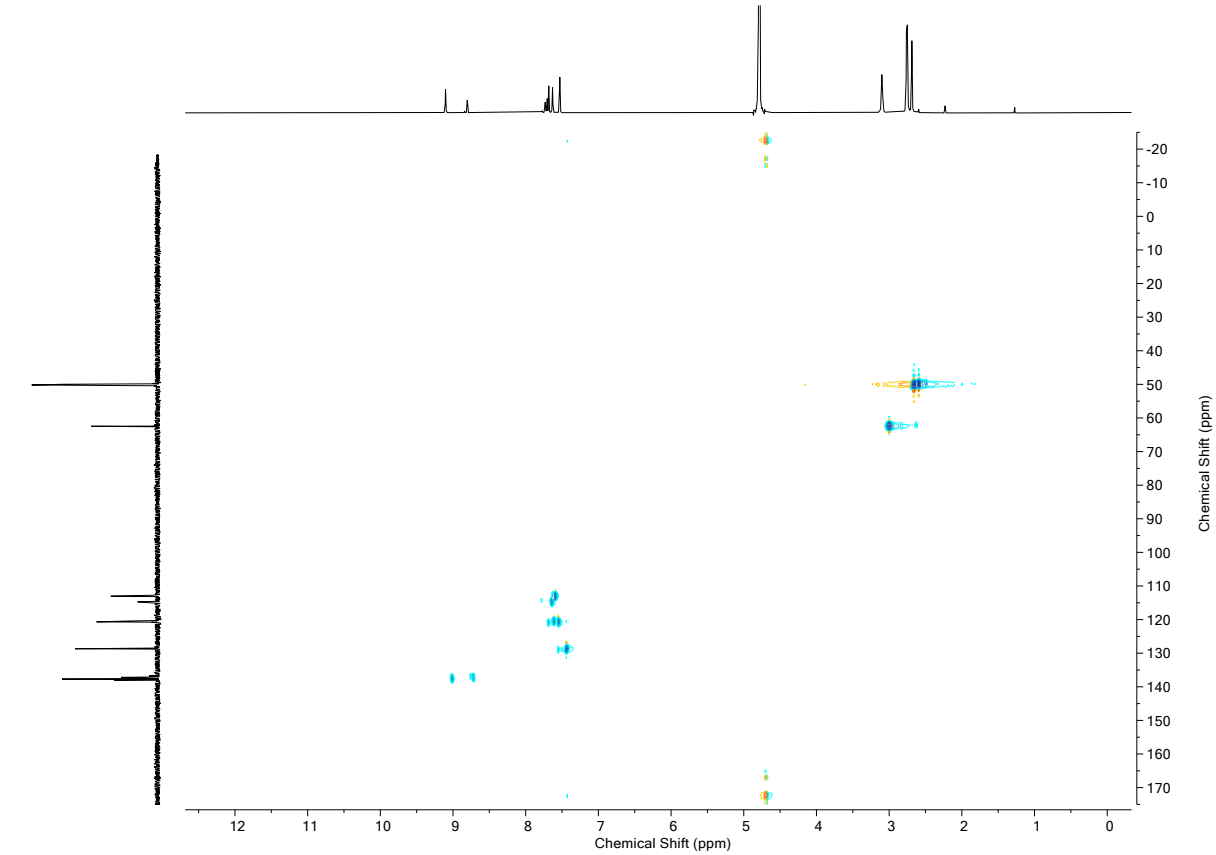

Figure S23: HSQC spectrum of **Cage** (D_2O).

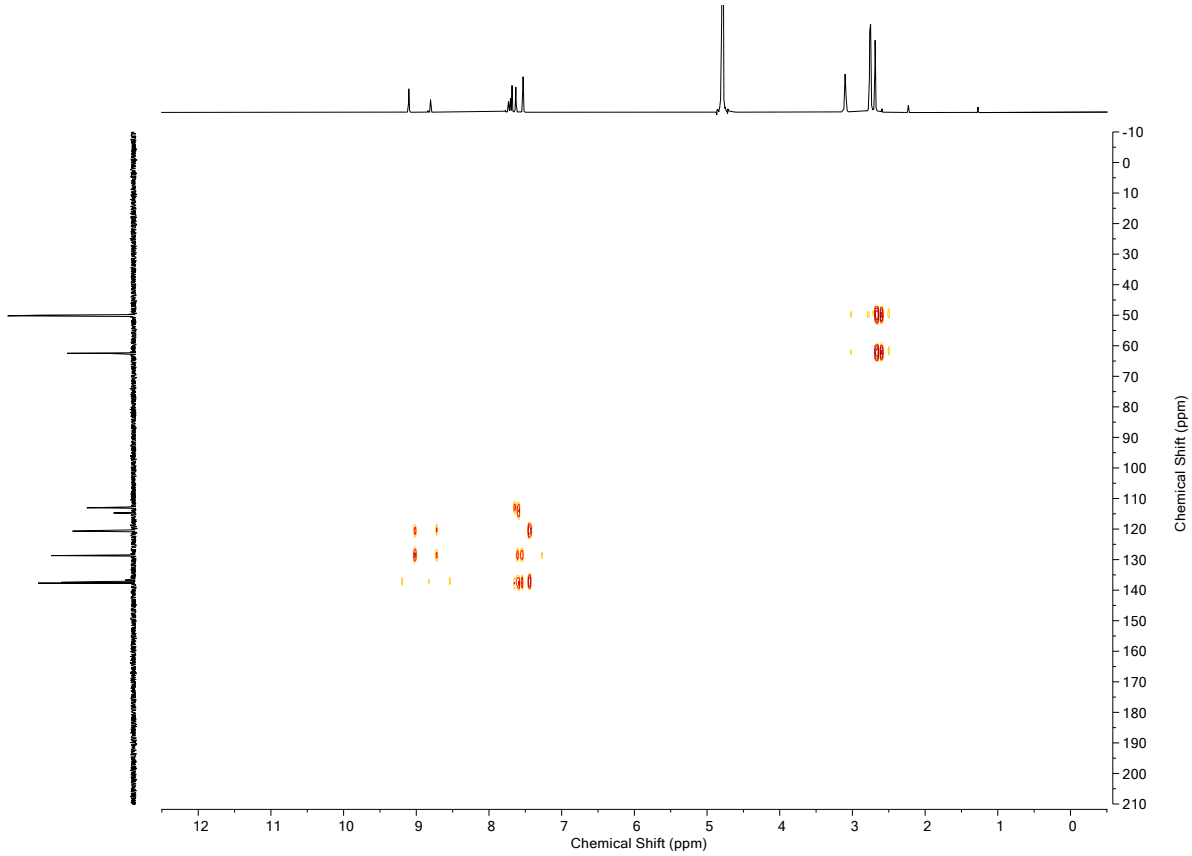

Figure S24: HMBC spectrum of **Cage** (D_2O).

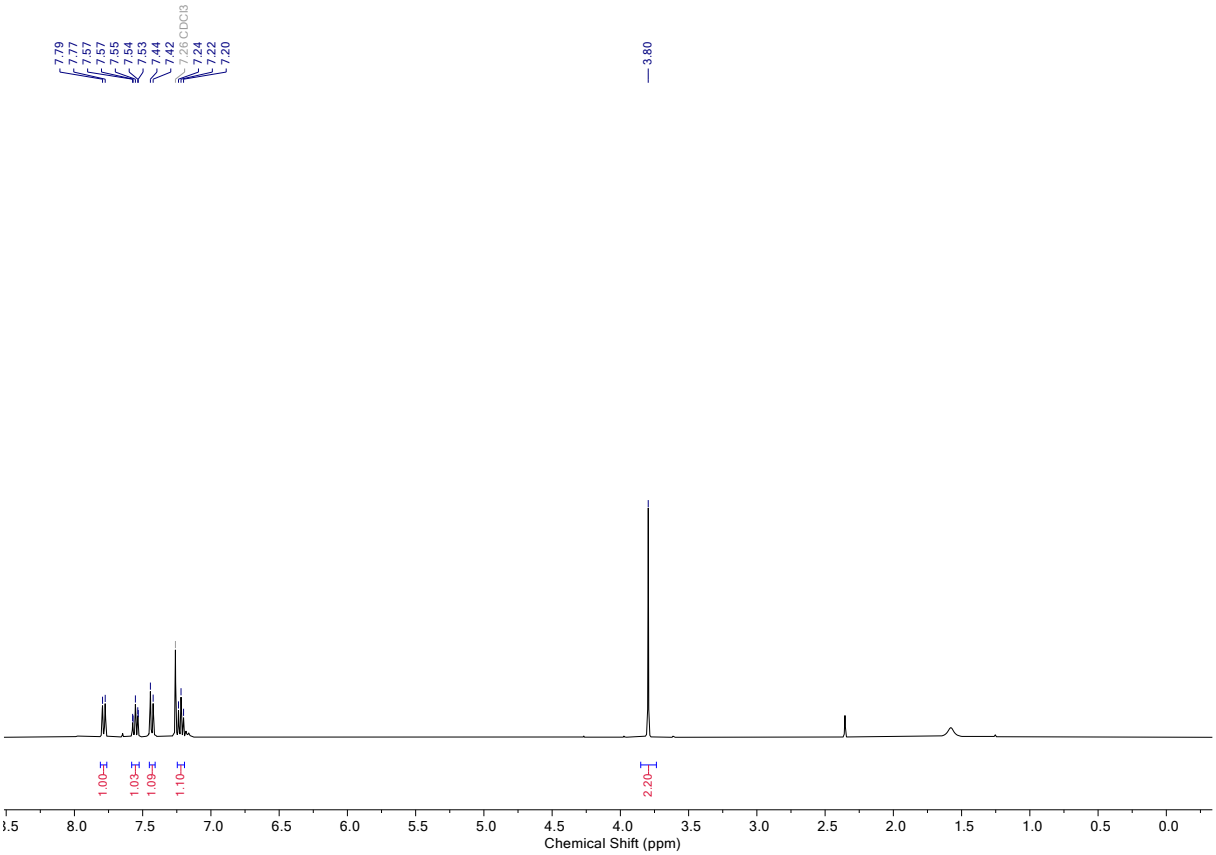

Figure S25: ^{1}H NMR spectrum of benzo[*b*]thiophen-3(2*H*)-one ($CDCl_3$).

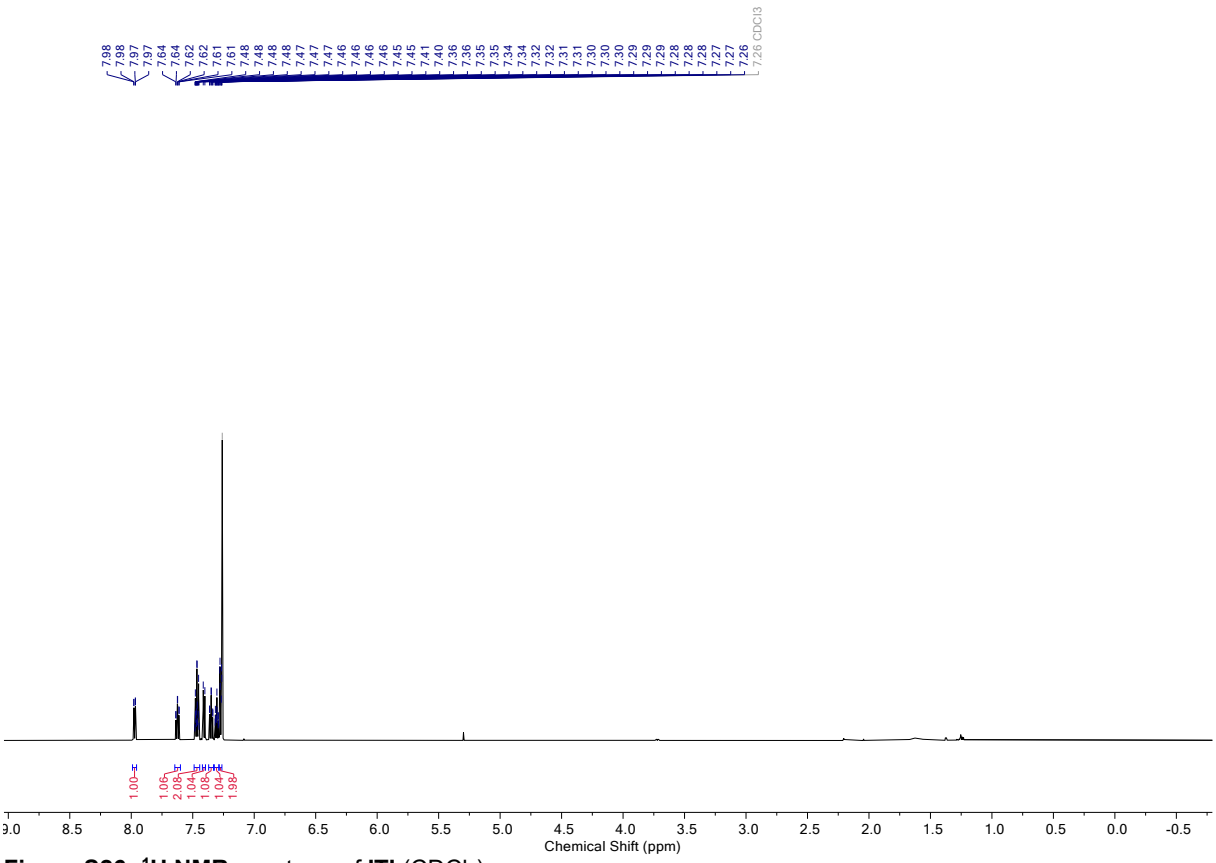

Figure S26: ^{1}H NMR spectrum of **ITI** ($CDCl_3$).

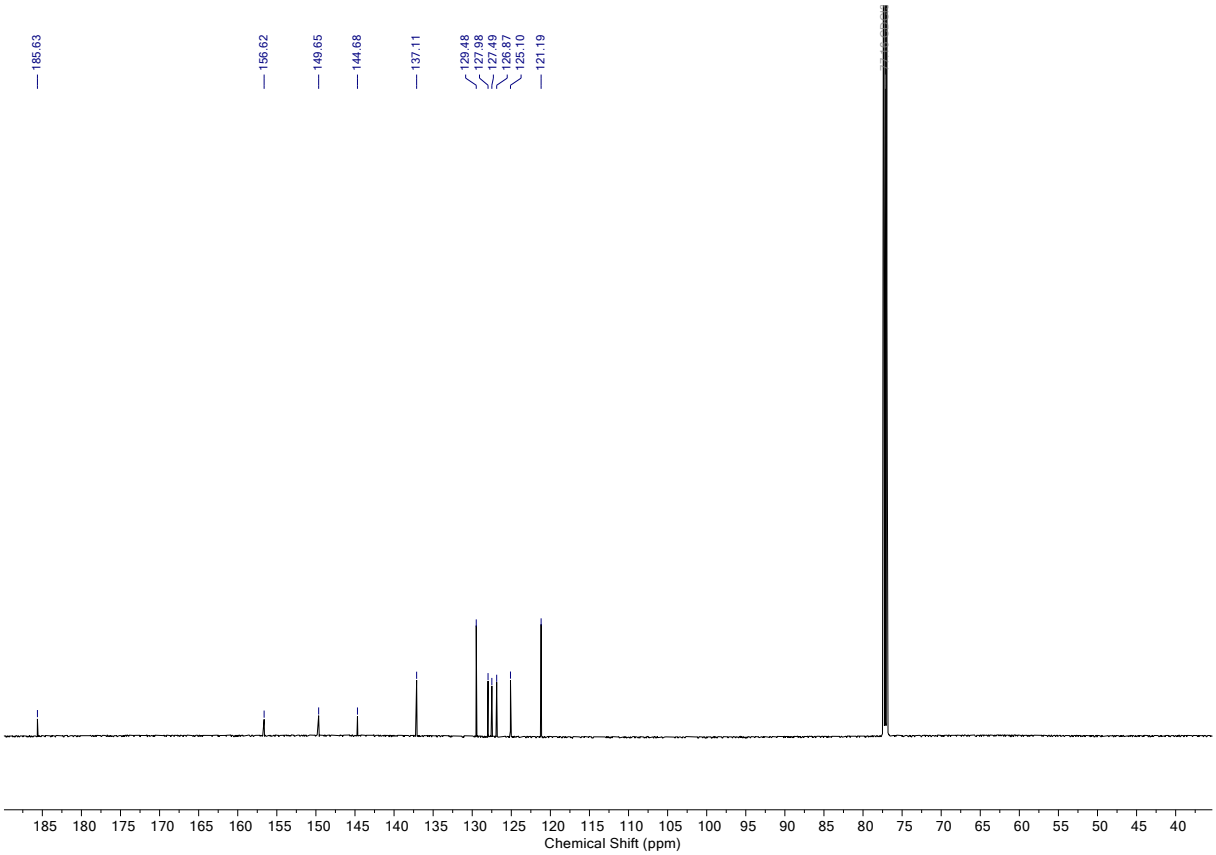

Figure S27: ^{13}C{^{1}H} NMR spectrum of **ITI** ($CDCl_3$).

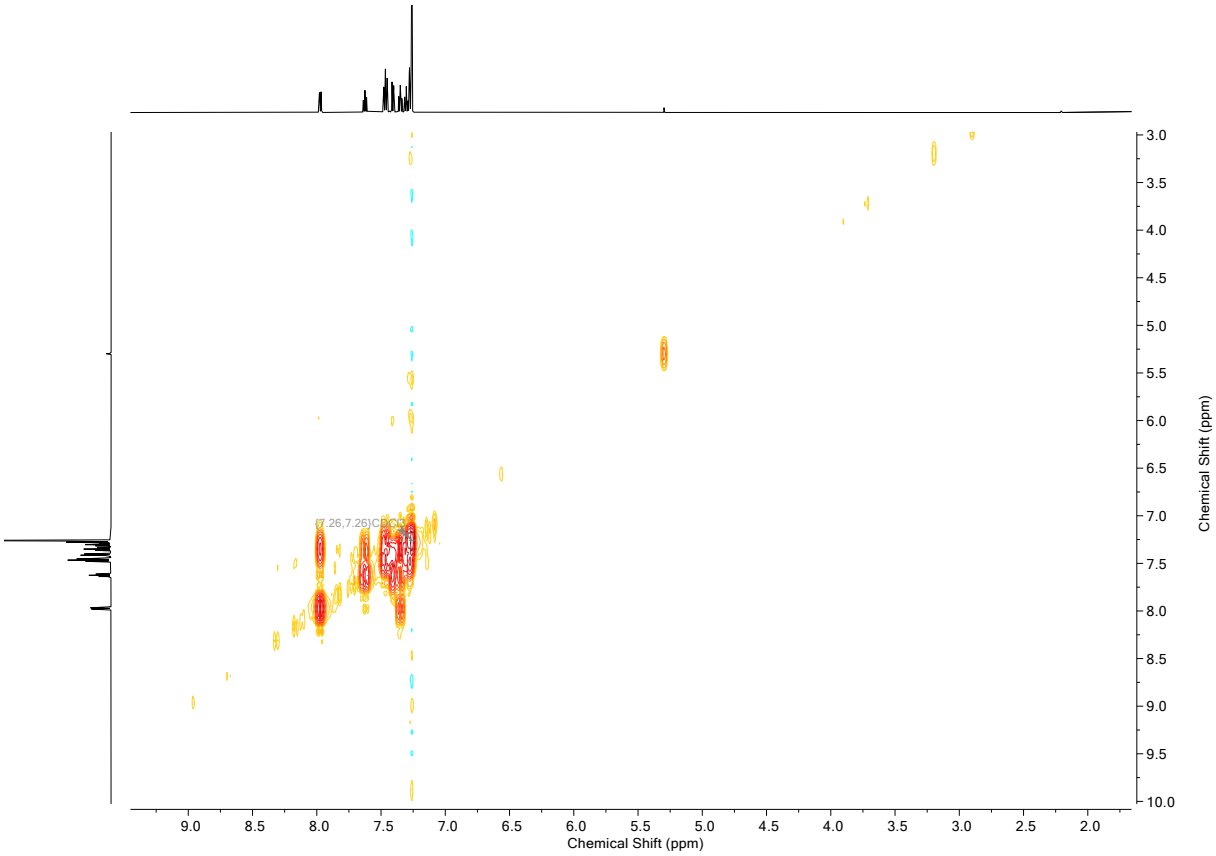

Figure S28: COSY spectrum of **ITI** ($CDCl_3$).

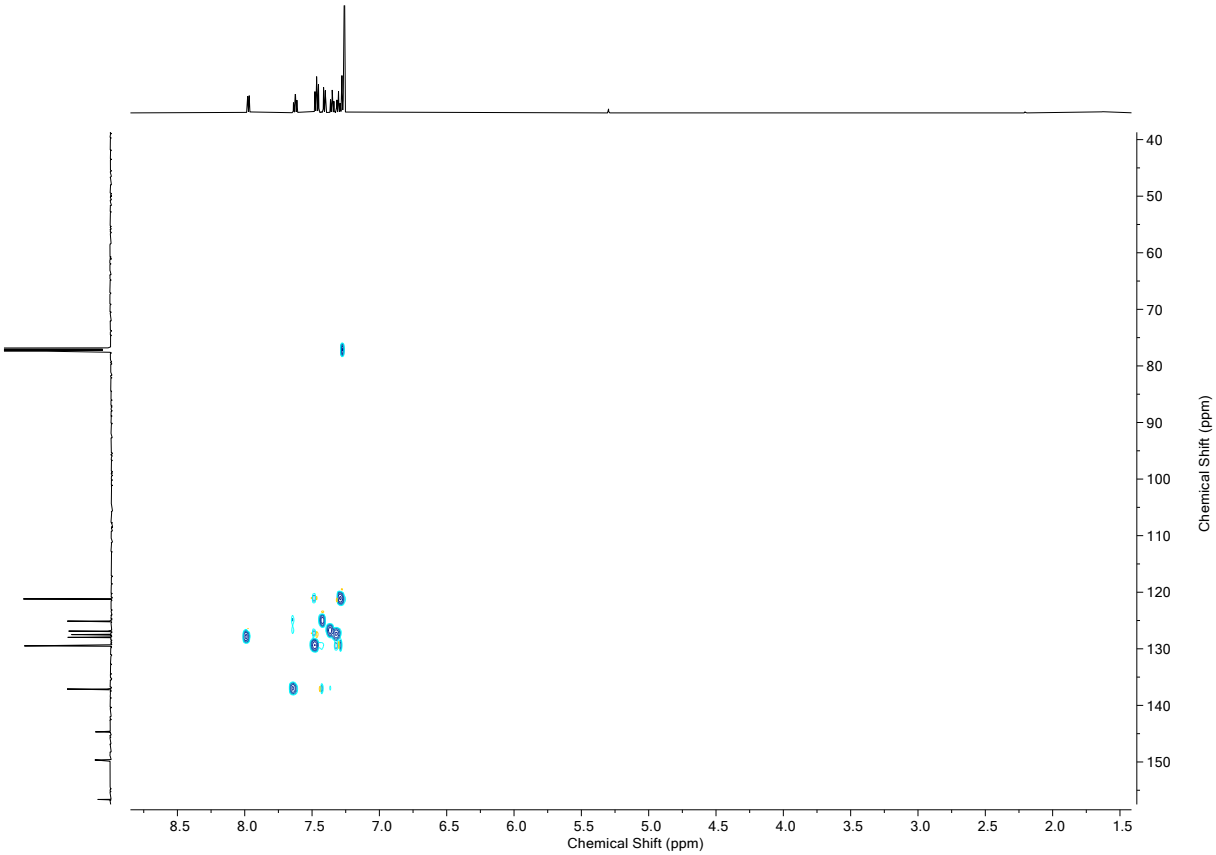

Figure S29: HSBC spectrum of **ITI** ($CDCl_3$).

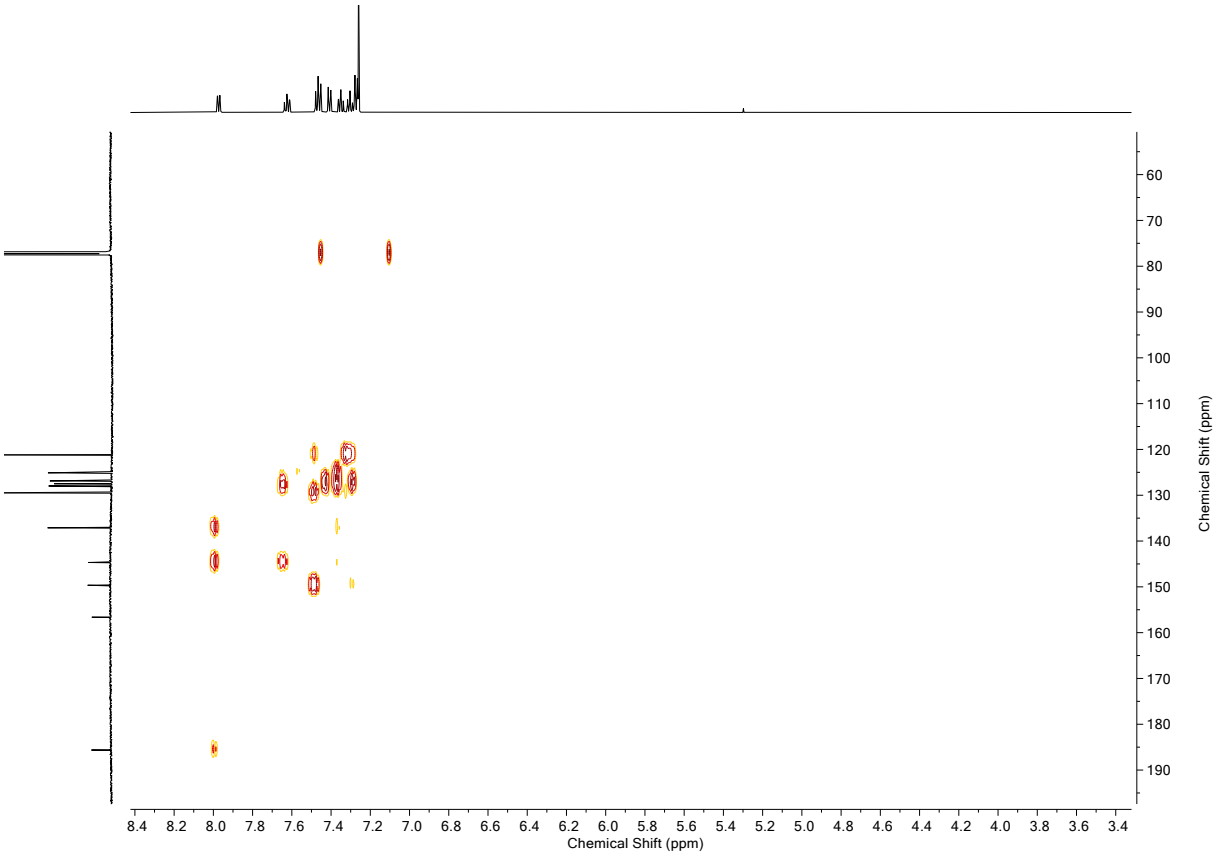

Figure S30: HMBC spectrum of **ITI** ($CDCl_3$).